Journal of Structural Geology, Vol. 14, No. 8/9, pp. 1079 to 1100, 1992
Printed in Great Britain

0191-8141/92 $05.00+0.00

Microstructural and crystal fabric evolution during shear zone formation

G. E. LLOYD

Department of Earth Sciences, University of Leeds, Leeds LS2 9JT, U.K.

R. D. LAW

Department of Geological Sciences, Virginia Polytechnic Institute and State University, Blacksburg, VA 24061, U.S.A.

D. MAINPRICE

Laboratoire de Tectonophysique, USTL, Place Eugene Bataillon, 34095 Montpellier Cédex 05, France

and

J. WHEELER

Department of Geological Sciences, University of Liverpool, Liverpool L69 3BX, U.K.

(*Received* 6 *September* 1991; *accepted in revised form* 28 *April* 1992)

Abstract—The microstructures and crystal fabrics associated with the development of an amphibolite facies quartzo-feldspathic mylonitic shear zone (Torridon, NW Scotland) have been investigated using SEM electron channelling. Our results illustrate a variety of microstructures and fabrics which attest to a complex shear zone deformation history. Microstructural variation is particularly pronounced at low shear strains: significant intragranular deformation occurs via a domino-faulting style process, whilst mechanical incompatibilities between individual grains result in characteristic grain boundary deformation accommodation microstructures. A sudden reduction in grain size defines the transition to medium shear strains, but many of the boundaries inherited from the original and low shear strain regions can still be recognized and define distinctive bands oriented at low angles to the shear zone margin. Grains within these bands have somewhat steeper preferred dimensional orientations. These domains persist into the high shear strain mylonitic region, where they are oriented subparallel to the shear zone margin and consist of sub-20 μm grains. The microstructures suggest that the principal deformation mechanism was intracrystalline plasticity (with contributions from grain size reduction via dynamic recrystallization, grain boundary migration and grain boundary sliding). Crystal fabrics measured from the shear zone vary with position depending on the shear strain involved, and are consistent with the operation of several crystal slip systems (e.g. prism, basal, rhomb and acute rhomb planes) in a consistent direction (probably parallel to *a* and/or *m*). They also reveal the presence of Dauphine twinning and suggest that this may be a significant process in quartz deformation. A single crystal fabric evolution path linking the shear zone margin fabric with the mylonitic fabric was not observed. Rather, the mylonitic fabric reflects the instantaneous fabric which developed at a particular location for a particular shear strain and original parental grain orientation. The mature shear zone therefore consists of a series of deformed original grains stacked on top of each other in a manner which preserves original grain boundaries and intragranular features which develop during shear zone evolution. The stability of some microstructures to higher shear strains,the exploitation of others at lower shear strains, and a continuously evolving crystal fabric, mean that the strain gradient observed across many shear zones is unlikely to be equivalent to a time gradient.

INTRODUCTION

THE crystallographic fabrics of shear zones which display the classic geometrical relationships between finite strain features (e.g. tectonic foliation, lineation, etc.) and shear zone boundaries with increasing heterogeneous shear strain due to bulk simple shear (Ramsay & Graham 1970, Ramsay 1980) should also be interpretable in terms of simple shear deformation. Previous work (e.g. Etchecopar 1977, Bouchez 1978, Burg & Laurent 1978, Bouchez *et al.* 1979) suggests that the dominant quartz slip direction ⟨*a*⟩ becomes aligned with the direction of bulk simple shear. The *a*-axis point maximum therefore indicates the shear direction, towards which the lineation (*X*) within the foliation plane (*XY*) progressively rotates. It also occupies the pole to a straight single girdle *c*-axis distribution. At very high shear strains, the *a*-axis maximum lies within the *XZ* plane at a very low angle to *X* and the *c*-axis fabric is oriented almost perpendicular to *X*. Consequently, the crystal slip plane should be parallel to the macroscopic shear plane.

Studies of some shear zones (e.g. Burg & Laurent 1978, Simpson 1981, Schmid & Casey 1986) support these observations, although the angle between the *a*-axis maximum and the lineation is often greater than expected whilst the *c*-axis girdle is often kinked. Other, perhaps most, shear zones (e.g. Law *et al.* 1984, 1986, Platt & Behrmann 1986, Schmid & Casey 1986, Law 1987) depart from these simple relationships, which

suggests that either the crystallographic slip model is not strictly applicable (Mancktelow 1987) or the deformation was not simple shear (Platt & Behrmann 1986, Law 1987). Moreover, Wenk & Christie (1991) have argued that the above relationships are too general and that there is no reason why crystals should rotate into those orientations, particularly as most minerals have more than one slip system and the slip plane and slip direction are not necessarily unique. However, Law *et al.* (1990) have reported a detailed study of the microstructures and crystallographic fabrics of a mylonitic shear zone developed within a quartzo-feldspathic vein in Proterozoic gneiss (Torridon, NW Scotland) which appears to be one of the rare examples representing the 'ideal case'. The present paper provides further analyses of this shear zone.

It is often assumed that the increasing shear strain gradient observed from the margins to the centres of many shear zones is equivalent to a time gradient. Crystal fabrics measured along this gradient therefore should not only constrain the actual strain path but also indicate the deformation mechanisms and crystallographic slip systems active at different stages along the path and their contribution to the magnitude and symmetry of the finite kinematic framework. This is an attractive proposition, but demands that complete crystallographic fabrics are measured on the small scale (often not much greater than the scale of the grain size). The optical microscope universal stage is capable of operating down to perhaps the 30 μm scale, but only provides *c*-axis fabric data. X-ray and neutron diffraction texture goniometry measure all fabric elements but yield only bulk fabric diagrams rather than individual relationships, and are also difficult to apply on the local scale within an individual sample. Transmission electron microscopy (TEM) is capable of operating on the very fine scale and provides all fabric data, but is restricted to specimens <3 mm in size and hence often suffers from being unrepresentative. A solution is provided by the electron channelling (EC) mode of operation of the scanning electron microscope (SEM). This technique permits the investigation of complete crystal fabrics at discrete points along a shear strain gradient and also the observation of the associated microstructures.

In this contribution we apply the SEM/EC technique to the study of local crystallographic fabrics in order to determine the deformation history (active deformation mechanisms, crystal slip systems, strain path and kinematic framework) of the 'ideal' Torridon shear zone. We emphasize that our results augment rather than conflict with those obtained by Law *et al.* (1990).

TECHNIQUES

SEM electron channelling

Several different types of image can be obtained in the SEM from the incident electrons which are reflected (backscattered) from the target specimen. The most frequently used backscattered electron (BSE) image is based on variations in atomic number, commonly known as Z-contrast (e.g. Lloyd 1987). However, the SEM also provides two types of BSE image based on specimen crystallography due to the *electron channelling* effect (e.g. Joy *et al.* 1982, Lloyd 1987). These are known as orientation contrast and electron channelling patterns (ECP). In the former, variations in image contrast distinguish changes in crystallographic orientation (e.g. grains, subgrains, etc.) and hence reveal images of specimen microstructure. The latter are distinct configurations of image contrast bands which represent the orientation of the crystal structure at the point of beam incidence. It is a simple matter to switch between the two types of SEM/EC image and it is therefore possible to derive via ECP the crystallographic orientation (with an accuracy >1°) of individual microstructural elements (>1–5 μm in size) observed in orientation contrast images.

Individual ECPs are identified by comparison with the complete range of ECP configurations permitted by crystal symmetry and mineral structure (e.g. Lloyd & Ferguson 1986, Lloyd *et al.* 1987a,b). A computer simulation programme (CHANNEL) is now available (Schmidt & Olesen 1989) to assist SEM/EC crystallographic analysis. This programme represents each ECP in terms of an orientation matrix from which inverse pole figures and pole figures for *any* crystallographic direction can readily be constructed (Lloyd *et al.* 1991).

Crystal fabric representations

All the crystal fabric diagrams presented in this contribution were constructed from ECPs obtained from individual grains (or subgrains) via CHANNEL. However, trends or specific behaviours are often difficult to recognize in discrete data pole figures. To show such trends more clearly, we have adopted the contouring approach suggested by Lloyd *et al.* (1991) and used by Lloyd & Freeman (1991). The CHANNEL-derived crystallographic orientation matrix is used to calculate the three spherical Euler angles from which the *true* orientation distribution function or ODF (e.g. Wenk *et al.* 1988) for the fabric can be estimated. Pole figure diagrams for specific crystal directions, contoured in terms of multiples of the uniform distribution, are then derived from the ODF. We believe that this is a more rigorous approach than merely percentage contouring of the original discrete data pole figures because it provides a statistical estimation of the population orientation distribution, including regions where the orientation density is less than that expected for a uniform distribution. We have not therefore included the original discrete data pole figures.

Specimen description

Figure 1(a) is a schematic drawing of an *XZ* section hand specimen of the Torridon shear zone, NW Scot-

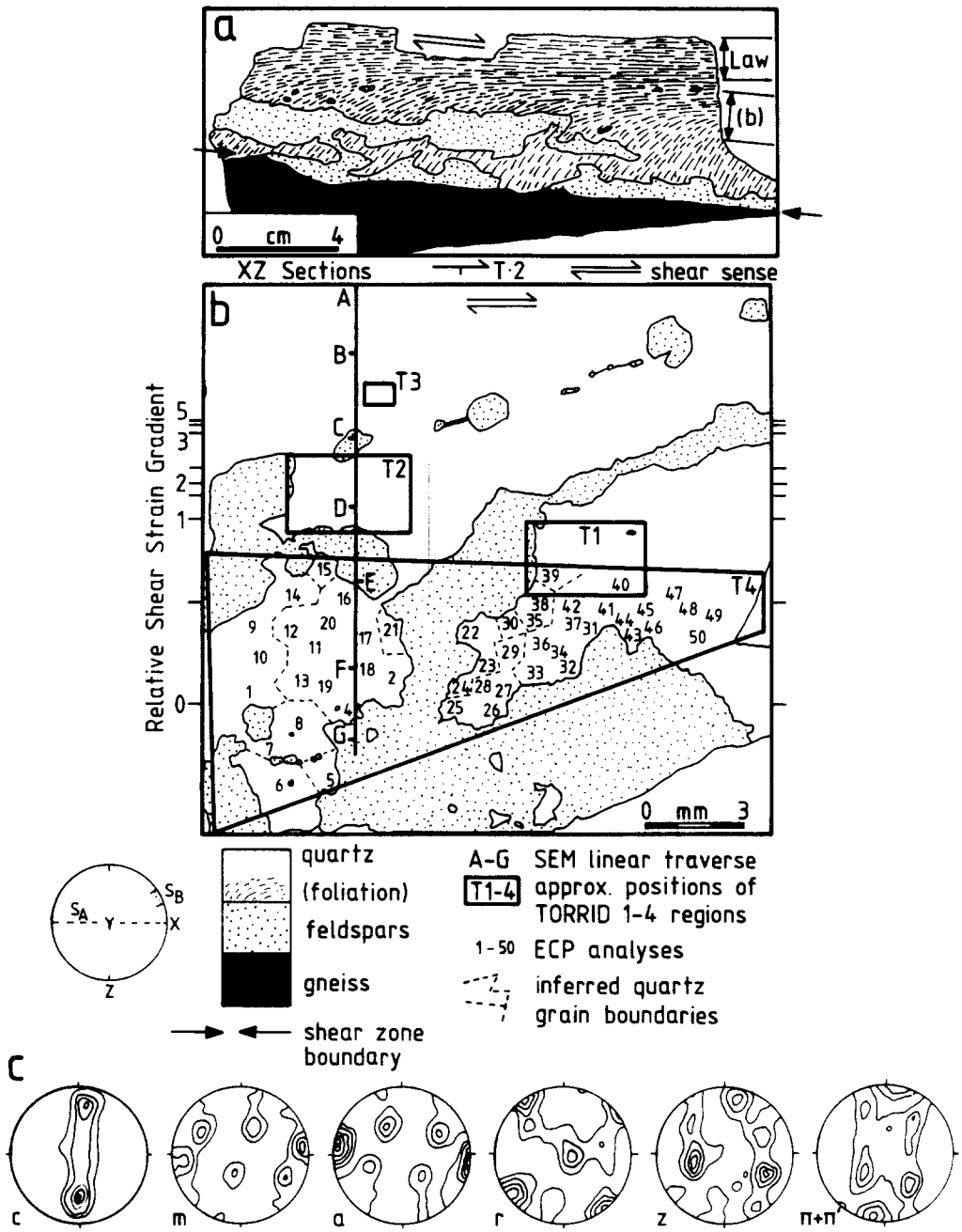

Fig. 1. (a) Schematic representation of an XZ section hand specimen of the Torridon shear zone (based on Law *et al.*, 1990, fig. 1a). The shear strain gradient region sampled by the SEM specimen is shown; note that it contains a complete section from the shear zone wall rock to the mature shear zone, and is also adjacent to the specimen used by Law *et al.* (1990). (b) Schematic diagram based on an SEM atomic number (Z) contrast photo-mosaic of the entire SEM specimen. Note the positions of the local microstructural and crystal fabric studies (T1–4); the continuous linear traverse (A–G) (Fig. 2); and the individual grains (only about 14 were recognized) and locations from which ECPs were obtained in the margin and lowest shear strain regions of the shear zone. The *relative* shear strain (γ) gradient, based on the reorientation of feldspar bands, is indicated along the left margin. The overall specimen-crystal co-ordinate system used by Law *et al.* (1990) and in this study is also shown (X, lineation; Z, pole to mylonitic foliation, S_A; Y, mutually perpendicular; S_B, range of dynamically recrystallized quartz grain shape alignment). (c) Summary of the X-ray texture goniometry derived crystallographic fabrics measured from the mature region of the Torridon shear zone by Law *et al.* (1990, fig. 4). Minimum(interval)maximum contour intervals (multiples of uniform distribution): c, 1(2)9; m, a, r, z and $\pi + \pi'$, 1(2)7.

land, (where X is the lineation direction, Z is perpendicular to the mylonitic foliation, and Y lies within the foliation perpendicular to X; use of X, Y and Z does not implicitly assume parallelism with the finite strain axes, Law *et al.* 1990). The shear zone margin consists of coarsely crystalline quartz and feldspar, whilst the shear zone centre is a typical mylonite consisting mainly of quartz with an intensely developed foliation and lineation (Law *et al.* 1990, fig 1b). The mylonitic quartz microstructure consists of alternating domains of equant fine grains (<5 μm), defining a mylonitic foliation subparallel to the XY plane (S_A of Law *et al.* 1990), and elongate coarse grains (40–70 μm) aligned oblique to S_A (S_B of Law *et al.* 1990). Boundaries between these

domains are parallel to S_A, whilst feldspar fragments are stretched out between S_A and S_B. The foliation initiates at a high angle to the shear zone margin, but within ~1 cm has curved into sub-parallelism with the margin. The curved trajectory of the mylonitic foliation indicates a dextral shear sense as viewed, which is consistent with all microstructures and crystal fabrics recorded by Law *et al.* (1990). No folding of the foliation is observed in this section plane.

The approximate relative positions of the specimens used in this study and by Law *et al.* (1990) are indicated in Fig. 1(a). Whereas the latter study sampled only the mature shear zone microstructure, our specimen includes a complete and representative microstructural section from the shear zone margin to the mature region. Thus, in this single specimen, we should be able to sample via SEM/EC the complete range of microstructures and crystal fabrics involved in the formation of this shear zone.

Figure 1(b) is a tracing from an SEM Z-contrast photo-mosaic of the whole specimen and indicates the positions of the local microstructural and crystal fabric studies described below. In particular, we emphasize that the shear zone margin in this specimen consists of relatively few large grains (about 14, as indicated by ECP analysis—see below). Although the shear zone is mainly quartz, its wall rock is dominated by discontinuous feldspathic bands which have been progressively rotated and boudinaged into parallelism with the mylonitic shear zone foliation (S_A). We assume that the angle (α) made by the feldspar bands with the shear zone margin represents their original orientation prior to shear zone initiation. The progressive rotation (α') of these bands towards S_A may therefore provide a *relative* estimate of shear strain (γ) using the equation (e.g. Ramsay 1967): $\cot\alpha' = \cot\alpha + \gamma$ (assuming $\gamma = 0$ where the bands intersect the margin, irrespective of the actual angle of contact). This relative shear strain gradient is indicated in Fig. 1(b), and offers a means of comparing microstructural and crystal fabric development with shear strain.

We have made a complete SEM/EC orientation contrast linear traverse across the specimen (Fig. 2). This traverse was made at ~250 times magnification, resulting in an as-seen length of ~3.75 m compared to a real length of only 15 mm. It is obviously difficult to represent such a traverse here, but nevertheless we try to do so in order to illustrate the progressive microstructural evolution of the shear zone with increasing shear strain. Positions along the traverse are defined via the continuous millimetric scale along the right edge. We have augmented the linear traverse with observations made off-traverse (Figs. 3–6). These are also indicated in Fig. 1(b).

Previous work

The crystallographic fabrics measured by Law *et al.* (1990) in the Torridon shear zone (summarized in Fig. 1c) are consistent with the bulk simple shear kinematic framework indicated by shear zone geometry. The α-axis fabric consists of a dominant point maximum oriented within the XZ plane at 9° to the lineation (X), subparallel to the bulk shear zone geometry and occupying a pole position to a single girdle c-axis fabric. Individual positions in the c-axis fabric skeleton are related by a common $\langle a\rangle$ direction coincident with this maximum. A simple set of relationships exists between shear zone geometry and the orientation of potential slip systems for different positions on the c-axis fabric skeleton. For the majority of grains considered, the acute negative rhomb $(\pi')[a]$ is almost perfectly aligned with the inferred simple shear kinematic framework. Such an alignment can be interpreted in terms of acute rhomb $[a]$ slip, although simultaneous basal $\langle a\rangle$ and negative rhomb $(z)\langle a\rangle$ slip are also indicated.

Although these crystallographic fabrics support a bulk simple shear kinematic framework (*sensu* Etchecopar 1977) for the formation of the Torridon shear zone, Law *et al.* (1990) emphasized that this does not justify an assumption that all mylonite zones form by simple shear deformation. Interpretation of individual deformation zones should be made on the basis of local information rather than general structural models. The analysis of crystallographic fabrics is important in such studies because (as Law *et al.* 1990, demonstrated) it helps to constrain the active deformation mechanisms (including crystallographic slip systems), the magnitude and symmetry of the finite strain, and the strain path and kinematic framework (see review by Schmid 1982). Unfortunately, it is usually difficult to isolate the influence of each of these factors on fabric development. Indeed, Law *et al.* (1990) adopted the traditional approach and confined their observations to the mature shear zone where a strong crystallographic fabric had already become established. Such regions probably represent the highest shear strains where most deformation and associated displacements have been accommodated, but consequentially they offer little potential for deriving the complete strain (deformation) path or for determining deformation mechanisms which may have been active earlier. We have therefore attempted to derive the deformation path for the Torridon shear zone by using SEM/EC to investigate both the microstructural and crystallographic evolution. Our approach assumes that the shear strain gradient from margin to centre is equivalent to a time gradient, but this is an assumption which will be tested by our investigation.

MICROSTRUCTURAL EVOLUTION

The SEM/EC linear traverse (Fig. 2) illustrates a variety of microstructures, most of which can be considered in terms of increasing shear strain. For the purposes of this description, we shall define our microstructural observations into *low* ($\gamma < 2$), *medium* ($\sim 2 < \gamma < 5$) and *high* ($\gamma > 5$) relative shear strains. Thus, if the spatial distribution of microstructures across the shear zone is equivalent to a time sequence, then the

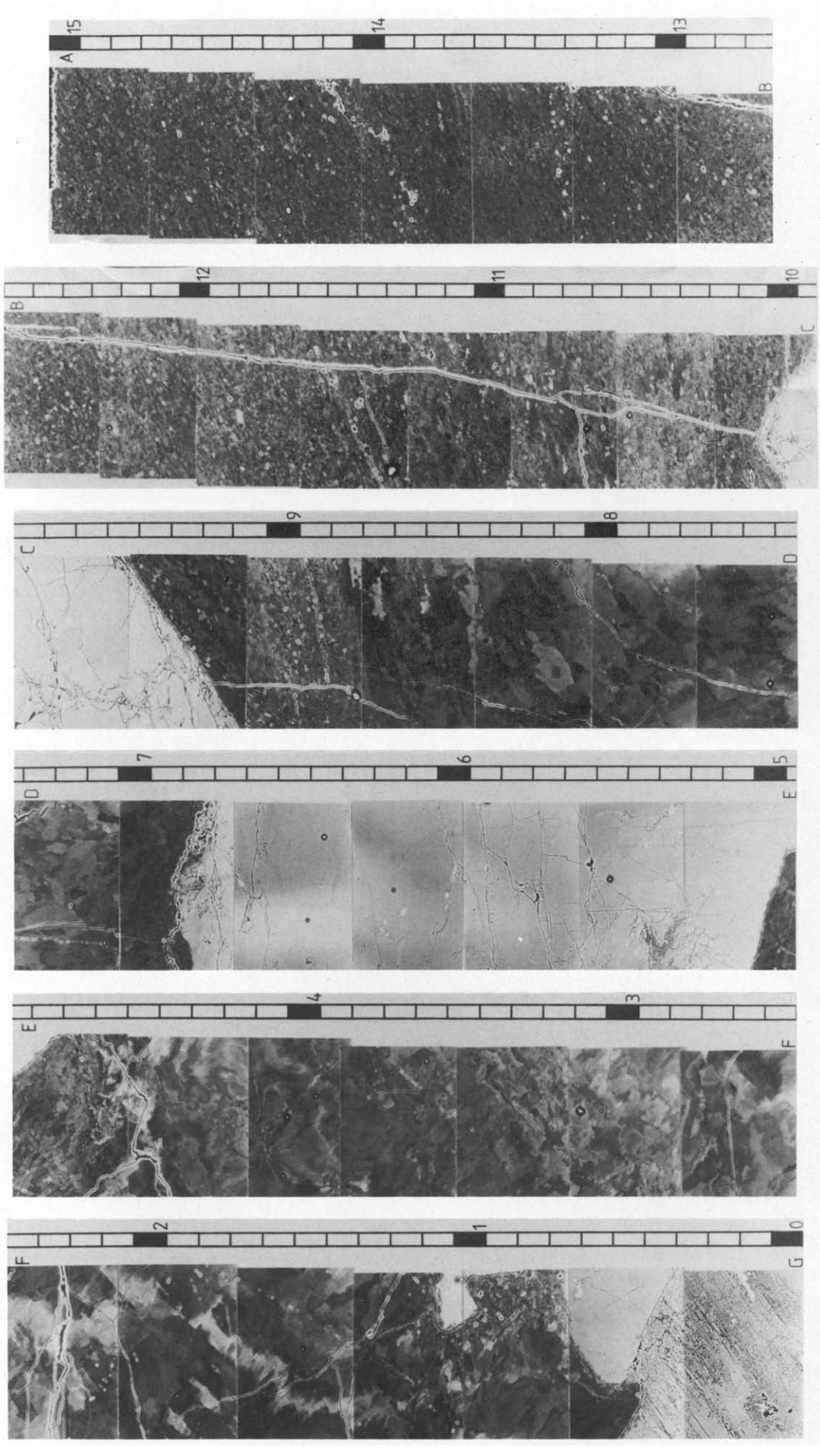

Fig. 2. SEM/EC orientation contrast image linear traverse (A–G; see Fig. 1b for location) across the specimen showing the progressive microstructural development of the Torridon shear zone from margin to mature mylonite. The large, bright contrast regions are feldspars. Note the millimetric scale on the right edge for position. See text for full description.

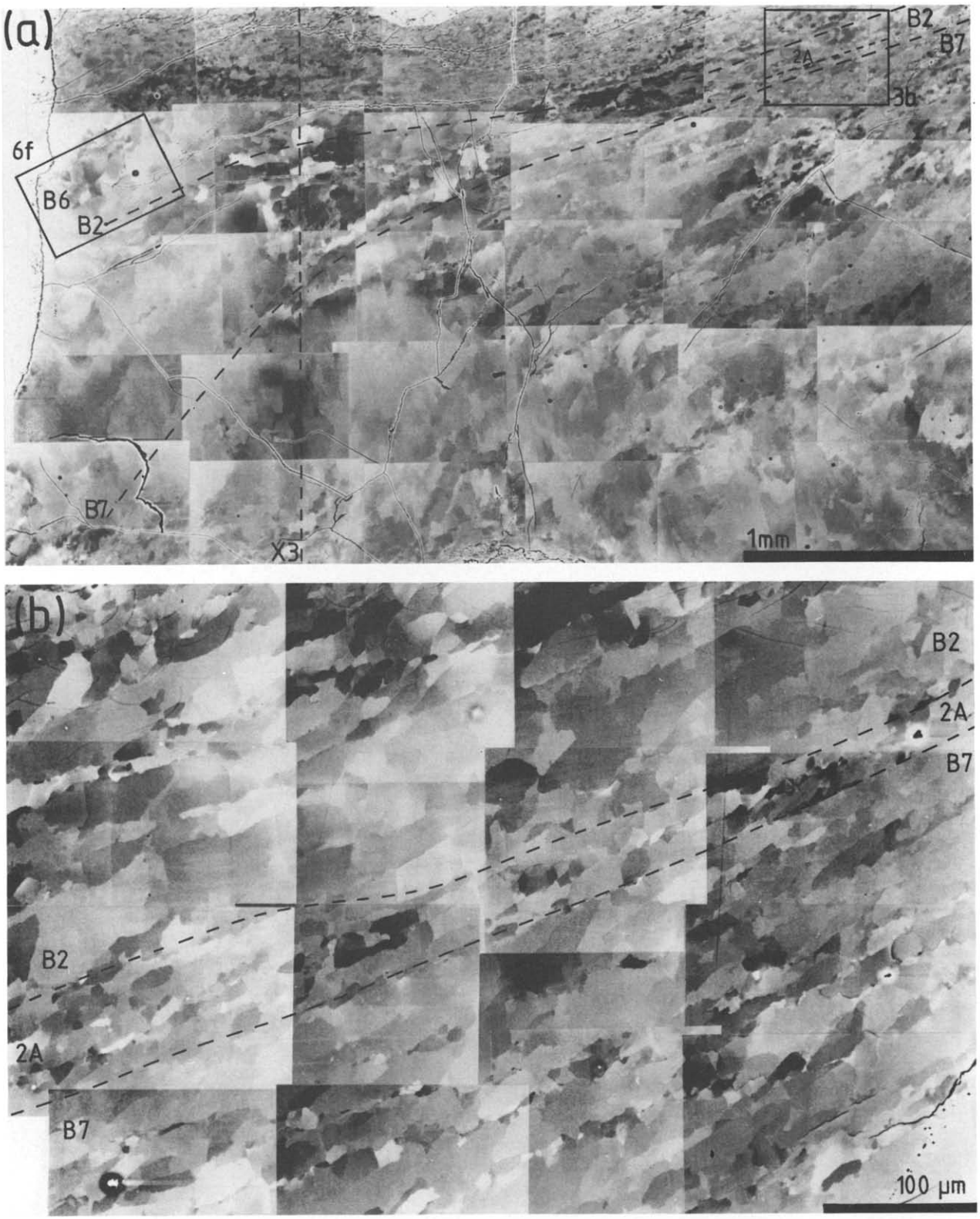

Fig. 3. SEM/EC orientation contrast image of intragranular microstructure typical of low shear strains (TORRID T2; see Fig. 1. for location). (a) Intragranular deformation often localizes on discrete linear (antithetic) features, resulting in elongate subgrains (containing smaller equant subgrains) progressively overturned in the (dextral) shear direction ('domino microstructure'), as indicated by ECP traverses B2 and B7. Grain-size reduction along these antithetic subgrain boundaries (e.g. ECP traverse 2A; see b) suggests that some degree of deformation localization has occurred along them. The upper part of the image shows the sudden reduction in grain size which marks the transition to the medium shear strain region. Also shown are the positions of the ECP traverse parallel to Z (X3) and positions of (b) and 6(f) (solid boxes). (b) Detail of part of (a) showing the elongate subgrains (e.g. B2, B7) which develop between antithetic linear boundaries (e.g. 2A), and the deformation localization and subsequent grain-size reduction which develop along these boundaries. The resulting microstructure is one of alternating relatively coarse and relatively fine recrystallized grain–subgrain sizes.

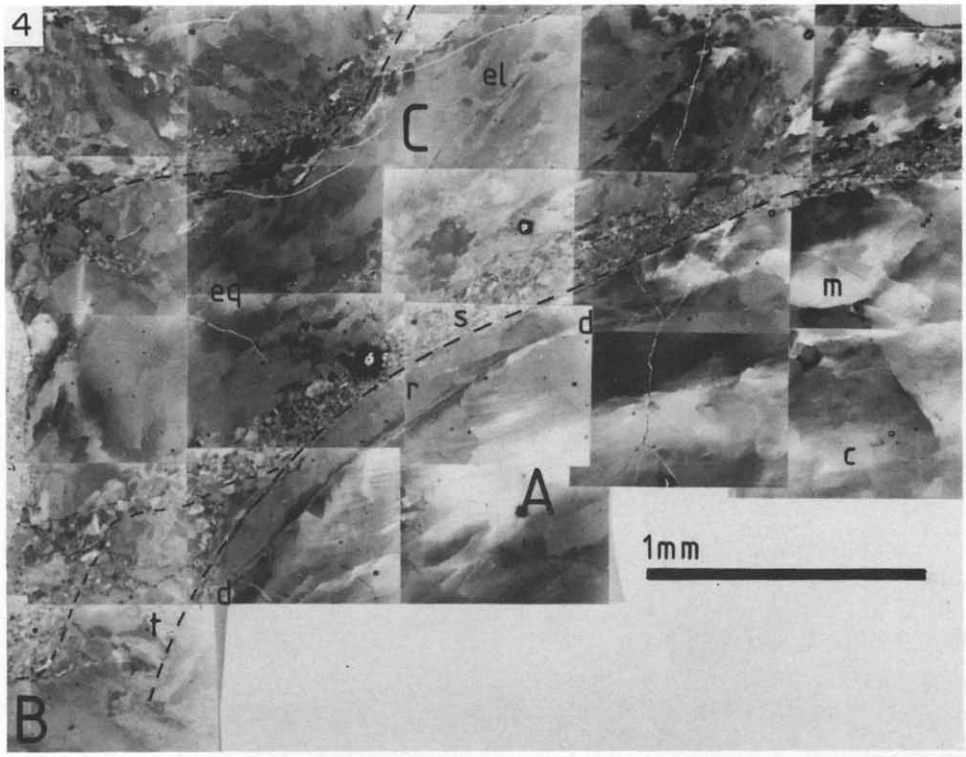

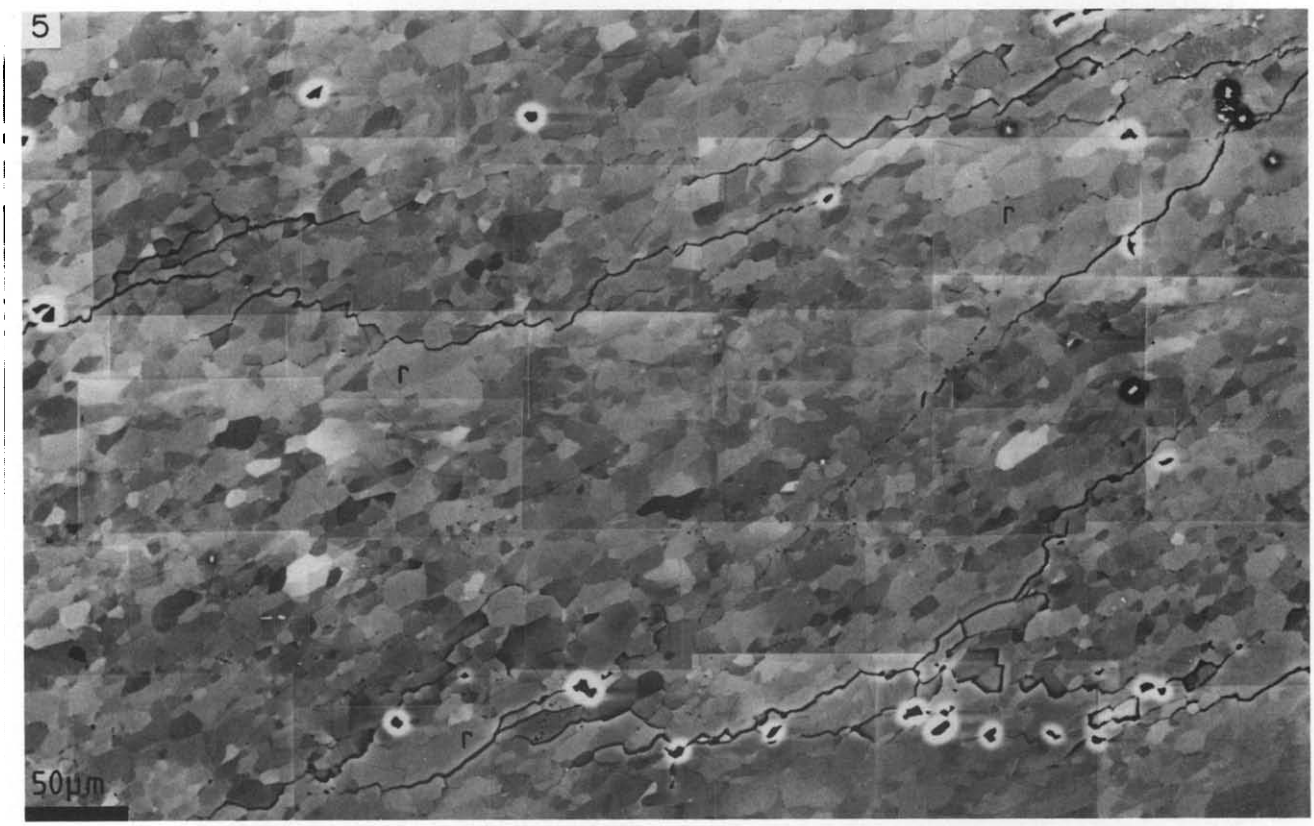

Fig. 4. SEM/EC orientation contrast image of different intragranular microstructures (TORRID T1; see Fig. 1 for location) observed at relatively low shear strains in three adjacent grains (A, B, C). Grain A exhibits a core region (c) of relatively large, equant subgrains surrounded by a mantle (m) of finer subgrains. Grain C exhibits alternating equant (eq) and elongate (el) subgrains, resulting in a localized domino microstructure. The differences in behaviour between these two grains are accommodated by the localization of deformation along and/or adjacent to the grain boundaries and the formation of distinct grain boundary microstructures: A, potential delamination of a surface region (r) along a grain boundary parallel shear band (d–d); C, intense subgrain–grain size reduction (s). Grain B exhibits a microstructure of alternating bright and dark contrasts (t), similar to that shown in Figs. 3(a, B6) and 6(f), interpreted as being due to Dauphine twinning.

Fig. 5. SEM/EC orientation contrast image of intragranular microstructures observed at high shear strains (TORRID T3; see Fig 1 for location). A true mylonite has developed consisting of a fine (<20 μm) grain size, although longer, 'ribbon' grains (r) are also observed. See Figs. 6(c)–(e) for other details of the mylonitic microstructure.

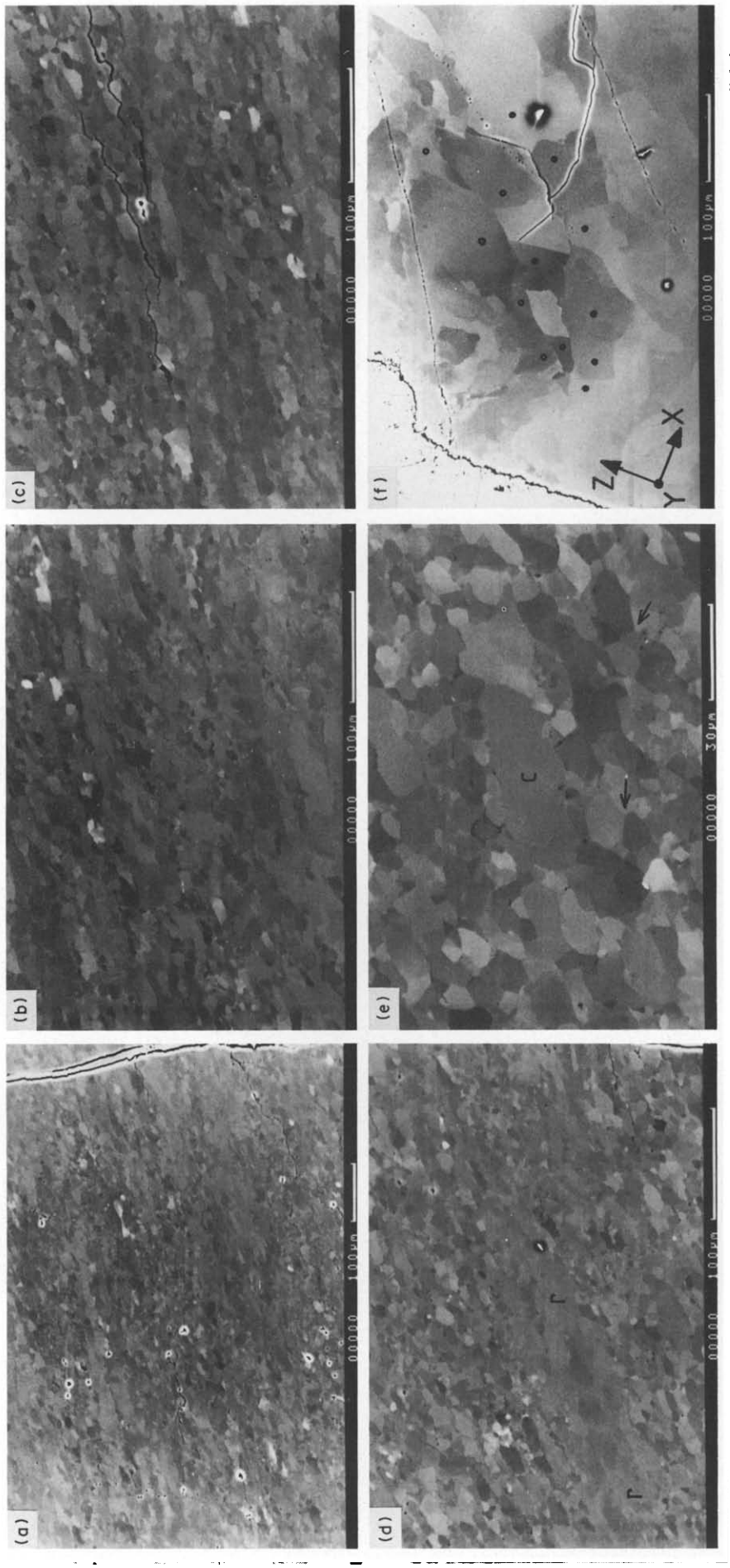

Fig. 6. High resolution SEM/EC orientation contrast images of shear zone microstructures. (a) Medium shear strains. Variation in grain size defining alternating bands. The bands have slightly different dimensional orientations (B_{PDO}) and either truncate against each other or pinch out gradually. (b) Medium shear strains. Grains within the bands show a preferred dimensional orientation (G_{PDO}) such that: $S_A < B_{PDO} < G_{PDO} < S_B$. Band boundaries are often decorated by finer grains. (c) High shear strains. Distinct domains with slightly different dimensional orientations (D_{PDO}) are defined by recrystallized grain-size variations. Truncation and/or pinching-out of these domains are less obvious than at lower shear strains, but do occur. Changes in grain preferred dimensional orientation (G_{PDO}) also occurs across domain boundaries, such that: $S_A \leq D_{PDO} < G_{PDO} \ll S_B$. (d) High shear strains. Longer, 'ribbon' grains (r) often persist from lower shear strains (note internal subgrains). (e) High shear strains. Straight grain boundaries and 120° grain boundary triple junctions (e.g. arrowed) provide evidence for local grain boundary migration and dynamic recrystallization, but there is little evidence of significant grain growth (although some grain coalescence, c, may have occurred). (f) Dauphine twinning microstructure observed at low shear strains (see Fig. 3a for location). Note the two scales of twinning: the smaller has boundaries subparallel to YZ; the larger has boundaries at ~45° to XY (i.e. S_A). Open circles, inferred host grain; solid circles, inferred twin grain.

SEM/EC linear traverse should include all the microstructural elements which were present at one time or another in the region now occupied by the mature mylonitic shear zone. The processes involved in the development of these microstructures contribute to the overall development of the shear zone and hence together define both the strain path and deformation history of the shear zone. The origin of these microstructures is central to any understanding of shear zone formation.

Low shear strain microstructures

Intragranular 'dominoes'. Many grains exhibit linear features which rotate in the (dextral) shear direction with increasing shear strain (Fig. 2, 1.2–1.9 mm, 7.0–8.4 mm; Fig. 3a). The orientation contrast changes across these features, which suggests that there is a (subtle) change in crystal orientation. There is also displacement across these features (in a sinistral shear sense) of areas with the same orientation contrast. Such displacements tend to decrease to zero in the direction of decreasing shear strain, where the linear features disappear (Fig. 3a). This suggests that these linear features accommodate movement between adjacent intragranular areas. A second set of (much shorter) linear features, oriented sub-normal to the first but otherwise with similar characteristics, is also observed (Fig. 2, 1.5–1.9 mm, 7.8–8.4 mm; Fig. 3a). We interpret both sets of linear features as subgrain boundaries.

The first set of linear subgrain boundaries results in an initial elongate subgrain microstructure which progressively rotates towards the shear direction (Fig. 3a). The second set results in an approximately equant subgrain microstructure (Fig. 2, 1.5–1.9 mm, 7.8–8.4 mm; Fig. 3). A subsidiary set of boundaries, subparallel to the first set, often develops subsequently within these equant subgrains, and may be followed by the development of a subsidiary set of boundaries oriented subparallel to the second set (Fig. 3). This cyclical development of displacement accommodating subgrain boundaries results in a progressive reduction in subgrain–grain size, accompanied by a continual change in shape (Fig. 7a).

We believe that the linear subgrain boundaries develop to accommodate intragranular deformations necessarily imposed on individual grains by the bulk simple shear framework. The significant observation is that consistent displacements occur across the boundaries, which we therefore consider to be analogous to 'domino fault' structures (e.g. Freund 1974, Mandl 1987). We envisage the following sequence of events (Fig. 7a). Initially, internal deformation is accommodated by block rotation on the long boundaries, resulting in antithetic (sinistral) displacement with respect to the bulk shear sense (perhaps in a similar manner to that envisaged by Lister & Williams 1983). However, this cannot continue indefinitely due to restrictions imposed both internally (e.g. by locking up of the system) and externally (e.g. by neighbouring grains). Thus, a second set of boundaries may develop with synthetic (dextral) displacement with respect to the bulk shear sense. But, these boundaries are subject to similar constraints, which may result in a switch back to the initial boundaries and/or the development of a second, minor, set of antithetic boundaries.

This behaviour of subgrain boundaries is similar to the accommodation of intragranular deformation by the operation of several different crystallographic slip systems. The subgrain boundaries probably represent zones of concentrated slip (e.g. deformation lamellae). As such, we could perhaps identify via SEM/ECP analysis specific crystal planes and directions which are parallel to these boundaries and hence infer equivalent slip systems, although it must be remembered that the boundaries are not necessarily normal to the XZ plane of the specimen.

As displacement continues on either set of linear subgrain boundaries, there is a tendency for much smaller (<10 μm) equant subgrains to develop along them (Fig. 3). Such grain sizes may accommodate further displacement by rotation and grain boundary sliding, which would represent a (local) additional and/or change in deformation mechanism.

Other intragranular microstructures. We have also observed several other distinctive intragranular subgrain microstructures. Some of the subgrains (e.g. Fig. 3) which develop between the initial antithetic boundaries are not formed by domino-style accommodation movements on smaller synthetic boundaries. Rather, they appear to represent conventional subgrains formed by rotation and/or the migration of boundaries. Such subgrains merely reflect internal deformation within the elongate subgrains as they suffer rotation and translation during the domino-style deformation process.

Other grains (e.g. Fig. 4, Grain A) exhibit a conventional core-and-mantle microstructure, consisting of relatively large and equant subgrains in the grain core surrounded by a mantle of finer subgrains. In contrast, an adjacent grain (Fig. 4, Grain C), which occupies the 'pressure shadow region' adjacent to a feldspar fragment, has a domino-style intragranular microstructure similar to that described above. However, regions with elongate subgrains and linear boundaries apear to be separated by regions with less well defined subgrains. This suggests intragranular partitioning of deformation and/or the operation of different crystal slip systems.

The variation (and complexity) of the intragranular microstructures means that these two adjacent grains have probably experienced different deformation histories. Presumably this is because there were not enough crystal slip systems available for homogeneous deformation. This results in incompatibilities in (shear) strains between the grains, which are accommodated along and/or adjacent to the grain boundaries. It is therefore significant that a distinctive microstructure, consisting of small (<10 μm) equant grains, is observed in the grain boundary region between grains A and C (Fig. 4). This microstructure forms a relatively sharp boundary with Grain A, but a rapidly increasing grain–

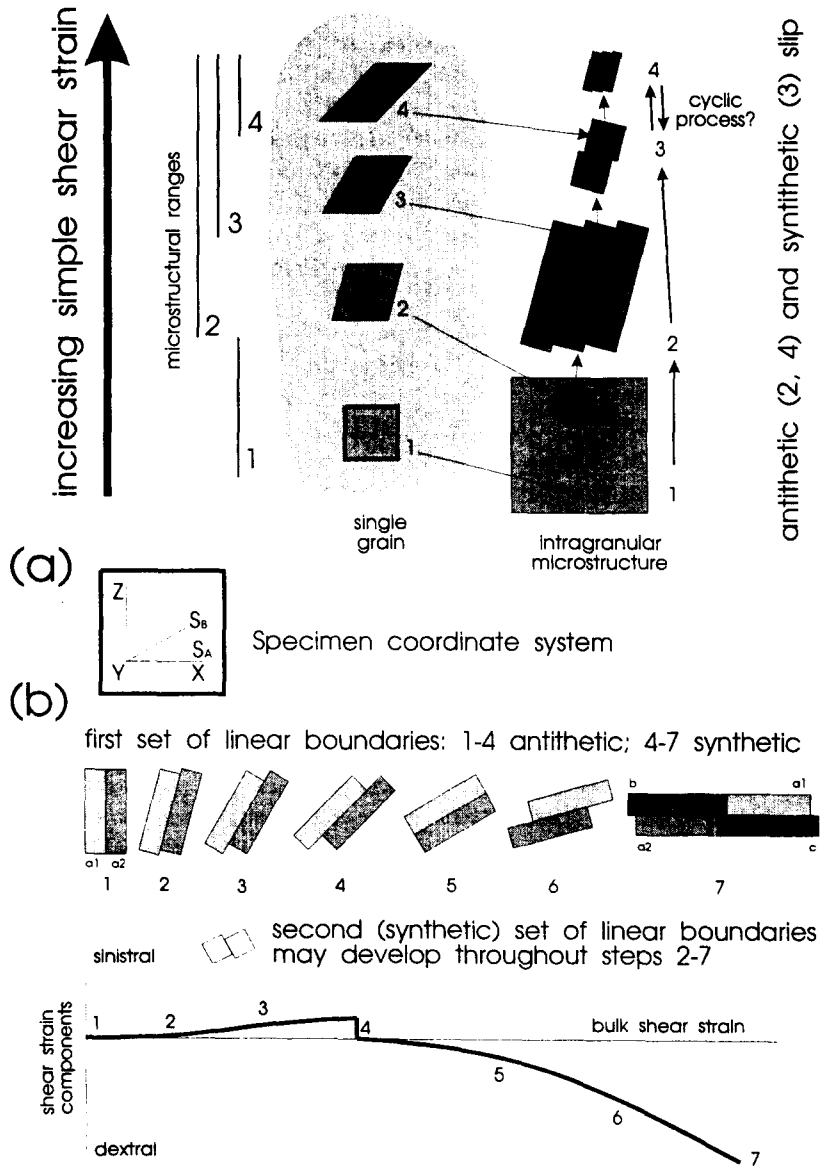

Fig. 7. Schematic illustration of the domino-faulting style of intragranular deformation at low shear strains (compare with Fig. 3a). (a) Individual grain microstructural behaviour, resulting in a variation in intragranular microstructures (1–4). 1, Undeformed grain. 2, Antithetic dominoes, resulting in elongate subgrains overturned in the bulk shear sense. 3, Synthetic, minor dominoes, resulting in equant subgrains. 4, A second set of antithetic dominoes, resulting in a smaller set of elongate subgrains overturned in the bulk shear sense. Steps 3–4 are obviously potentially cyclic. (b) Relationship between domino microstructure and deformation. Bulk dextral shear strain initially results in antithetic (sinistral) displacement between, and clockwise (dextral) rotation of, individual dominoes. With increasing rotation, the domino boundaries rotate towards the shear plane and the antithetic sinistral displacements diminish and are eventually replaced by synthetic (dextral) displacements. Eventually, the displacements can bring domains from different grains into juxtaposition. The bulk shear strain therefore consists of both dextral and sinistral components. Minor domino-style deformation within the major domino (elongate subgrains) structures can occur at any time in this sequence.

subgrain size is observed towards Grain C, which suggests that the grain boundary microstructure has developed predominantly from Grain C. In contrast, Grain A exhibits a thin surface region, separated from the mantle subgrains by a narrow zone of concentrated deformation (shear band or deformation lamellae?), which may represent an equivalent grain boundary microstructure. The fine grain size would be capable of both accommodating and further localizing deformation by grain boundary sliding processes, whilst it is possible that the thin surface region is being peeled off the rest of Grain A along the zone of concentrated deformation (i.e. in a manner similar to exfoliation or delamination?).

These observations suggest that at low shear strains different grains respond differently to the deformation, whilst maintaining the bulk rotations necessary for mechanical compatibility during shear zone formation. The net result of these processes is to form a network of narrow zones of significantly reduced grain–subgrain sizes which separate more coarsely grained–subgrained regions where the original characteristics of individual grains are preserved to higher shear strains. Thus, the general increase in shear strain and progressive micro-

structural development from the margin into the shear zone is replaced in detail by local variations, leading to local deviations of the shear strain gradient away from the time gradient.

Medium shear strain microstructures

A sudden overall decrease in grain size is observed across a plane subparallel to the shear zone boundary (Fig. 2, 8.8 mm; Fig. 3a). We define this plane as the transition from low to medium shear strains. Nevertheless, there remains a considerable variation in grain size within the medium shear strain region, with alternating relatively coarse- and relatively fine-grained bands (Fig. 2, 10.1.–11.4 mm; Figs. 6a&b). These bands have slightly different dimensional orientations (B_{PDO}), distributed between S_A and S_B, and either truncate against each other or pinch out gradually. The boundaries between bands may be decorated by small (<10 μm), equant recrystallized grains. The grains and subgrains within each band also tend to have a preferred dimensional orientation (G_{PDO}) between S_A and S_B, with larger grains having orientations closer to S_B. However, the internal G_{PDO} is not necessarily parallel to B_{PDO}, and in general the following relationship is observed: $S_A < B_{PDO} < G_{PDO} < S_B$.

We interpret these microstructures as representing the continued development, but also persistence, of the microstructures observed at low shear strains. The individual bands (Figs. 6a&b) are formed by the various boundaries (especially the linear elongate subgrain boundaries) which developed at lower strains. They have continued to rotate towards S_A with increasing shear strain. The rotation is accommodated, as we have already observed, along the boundaries in a manner analogous to domino-faulting (Fig. 7a). However, this means that the *local* shear sense across band boundaries should be sinistral (i.e. antithetic) rather than dextral (i.e. synthetic). As the bands rotate towards S_A (Fig. 7b), so do the boundaries; consequently the sinistral shear declines, to be replaced eventually by dextral shear. The change in shear sense potentially occurs when the boundaries develop an angle of ~45° to S_A. Once this is achieved, dextral displacements can increase rapidly such that initially adjacent bands from the same grain may decouple completely (Fig. 7b). They can therefore become adjacent to bands which originate either from other parts of the same grain with different initial microstructures, or from entirely different grains. Both situations result in rapid microstructural transitions and may explain the sudden decrease in grain size across a boundary subparallel to S_A which we have taken to represent the change from low to medium shear strains.

Alternative explanations for the sudden change in microstructure are (S.M. Schmid personal communication 1992): (1) inhomogeneous simple shear, with regions of higher strain bounded by regions of lower shear strain; and/or (2) the development of higher shear strain regions relatively late in the shear zone deformation history. Either alternative means that these microstructures are imposed upon, rather than inherited from, earlier states. This would invalidate completely any assumption that the shear strain gradient observed across the shear zone is equivalent to a time gradient which records the complete strain history. However, the microstructural evolution suggested above actually allows for the occurrence of inhomogeneous simple shear due to the juxtaposition of domains which have developed in isolation. The possibility of a late, high shear strain imprint is more difficult to distinguish, but would perhaps be expected to result in additional microstructures indicative of fracturing and cataclasis. These are not observed.

Localized intense grain size reduction by dynamic recrystallization was observed along linear subgrain boundaries in the low shear strain microstructure. It was suggested that these developed to accommodate further deformation along the boundaries via grain boundary sliding. A similar explanation is offered for the very small (<10 μm) equant grains observed in the same positions in the medium shear strain microstructure (Figs. 6a&b). Subsequent shear deformation may localize on these boundaries, resulting in localized zones of enhanced shear strain and displacement which herald the development of a penetrative high shear strain microstructure.

Although bulk deformation compatibility is maintained across the band boundaries, the internal microstructure of the bands reflects the initial crystal orientation and earlier subgrain microstructure of the parental grain, rather than the formation and evolution of the band-defining boundaries. These microstructures (Figs. 6a&b) therefore develop to a certain extent in isolation. We have already described the formation of equant subgrains via a second (synthetic) set of linear subgrain boundaries. This process obviously continues with increasing shear strain. Indeed, it may become dominant, with shear strain accommodated on these boundaries rather than the first (antithetic) set (Fig. 7b). The net result is a continuation of the progressive grain size reduction via dynamic recrystallization, with the variation in grain size across band boundaries explained by the juxtaposition of domains which occupy different stages in the same overall deformation path. Thus, the general increase in shear strain and progressive microstructural development from the margin into the shear zone is increasingly perturbed in detail by local variations, leading to more significant deviations of the shear strain gradient away from the time gradient.

High shear strain microstructures

The typical microstructure in this region consists of an essentially uniform fine (<20 μm) grain size (Fig. 2, 14.6 mm; Fig. 5), with many grains consisting of a few (typically 5–10 μm) subgrains (Figs. 6c–e). In detail, slight changes in grain size occur, usually across relatively sharp boundaries which define distinct domains (Fig. 6c). These are similar to the bands observed at

medium shear strains but are on a finer scale and have preferred dimensional orientations (D_{PDO}) closer to S_A (Fig. 2, 13.6–14.0 mm). The domains may truncate against each other (Fig. 2, 13.4 mm, 14.1 mm) or pinch-out (Fig. 2, 13.5 mm). The grains within the domains show a local preferred dimensional orientation (G_{PDO}) which changes slightly across the domain boundaries and in general is always slightly steeper than the associated D_{PDO}. Thus, the general relationship observed is: $S_A \leq D_{PDO} < G_{PDO} \ll S_B$.

We again prefer to interpret these boundaries as representing either original grain boundaries or intragranular boundaries formed at lower shear strains which continue to persist to high shear strains. However, the alternative explanations discussed in the previous section (i.e. inhomogeneous simple shear and/or the occurrence of localized high shear strains late in the deformation history) should again be mentioned.

Long (e.g. 300 μm), thin (e.g. <50 μm) 'ribbon' grains (Fig. 2, 13.6 mm; Fig. 6d) are also observed in the high shear strain microstructure. The origin of these grains is unclear. They may represent (our preference) the persistence of grains from lower shear strain regions. However, they may also represent either the coalescence of grains developed at the high shear strains and/or the anomalous growth (secondary recrystallization?) of some grains within the generally fine-grained microstructure (e.g. Fig. 6e).

The high shear strain microstructure appears to be stable. There is evidence (e.g. straight boundaries, 120° triple junctions) for local grain boundary migration (Figs. 5 and 6e), but this must obviously balance the internal strains. There is no evidence of significant grain growth (apart perhaps from the ribbon grains described above). Indeed, any change in grain size continues the progressive refinement trend with the formation of continuous narrow (~10 μm) bands oriented parallel to the shear direction, consisting of ultra-fine (<5 μm) grains (Fig. 2, 14.8 mm). These represent the further localization of deformation into thin bands parallel to the shear zone boundary and S_A.

The apparent stability of the high shear strain microstructure means that once it has formed, we can infer little more about the succeeding deformation history. Only the development of the localized shear bands parallel to S_A provides additional information. Thus, any time gradient across the shear zone effectively ends with the development of the high shear strain microstructure.

The deformation mechanism(s) active in this region are not immediately apparent from the microstructure. Displacements on the domainal boundaries, analogous to crystal slip, may account for much of the deformation as a continuation of the process depicted in Fig. 7(b). These will be abetted by the localization of deformation into shear zone parallel bands. The presence of subgrains in many of the grains proves that some intracrystalline plasticity has occurred. However, the fine grain size could also promote a change to penetrative deformation via grain boundary sliding processes, which would be capable of maintaining this microstructure to very high shear strains.

Effects of feldspar

We are principally concerned with the behaviour of quartz during the formation of the Torridon shear zone, but some comments on the deformation of the feldspars are appropriate. Feldspar generally behaves in a brittle manner during the evolution of this shear zone. Feldspar bands, oriented at an angle to the shear zone margin, are progressively rotated towards the mylonitic foliation and undergo boudinage resulting in fragment/grain size reduction with increasing shear strain (e.g. Figs. 1a&b and 2). We have also observed intragranular microstructures (e.g. subgrains) and the growth of metamorphic minerals (e.g. zoisite) associated with feldspar deformation. Perhaps the most significant aspect of the presence of feldspar in the shear zone is that it tends to perturb the deformation in the adjacent quartz matrix, leading to anomalous and localized microstructures (see also discussions by Hanmer & Passchier 1991). In particular, the rotation (vorticity) of feldspar fragments may impose locally an opposite (sinistral) sense of shear on the dextral shear zone microstructure. This effect is most obvious at low shear strains where it progressively overprints the bulk dextral shear microstructure to produce initially an anomalous microstructure with no apparent shear sense criteria and eventually a sinistral deflection. At higher shear strains the antithetic effect of feldspar rotation does not produce quartz microstructures with opposite shear senses, although it may be responsible for an apparent enhancement or reduction in the shear strain observed.

CRYSTALLOGRAPHIC FABRICS

We have described in detail in the previous sections the microstructural evolution of the Torridon shear zone. However, a complete understanding of shear zone formation must also include an appreciation of the crystallographic fabrics associated with these microstructures. Our microstructural analysis suggests that this should be performed on the scale of the smallest component microstructural elements (i.e. the decreasing grain–subgrain size). The SEM/ECP technique is particularly suited to these demands. We therefore now present an investigation of the crystal fabrics corresponding to the quartz microstructures observed along the increasing shear strain gradient. The locations of these fabrics are shown in Fig 1(b).

Original fabric (TORRID-4)

The grain sizes in the margin and lowest shear strain regions of the shear zone (Fig. 1b) vary considerably but can be quite large (e.g. >3 mm). We have been able to collect almost the complete fabric of these regions by traversing over the region in the SEM/ECP mode and

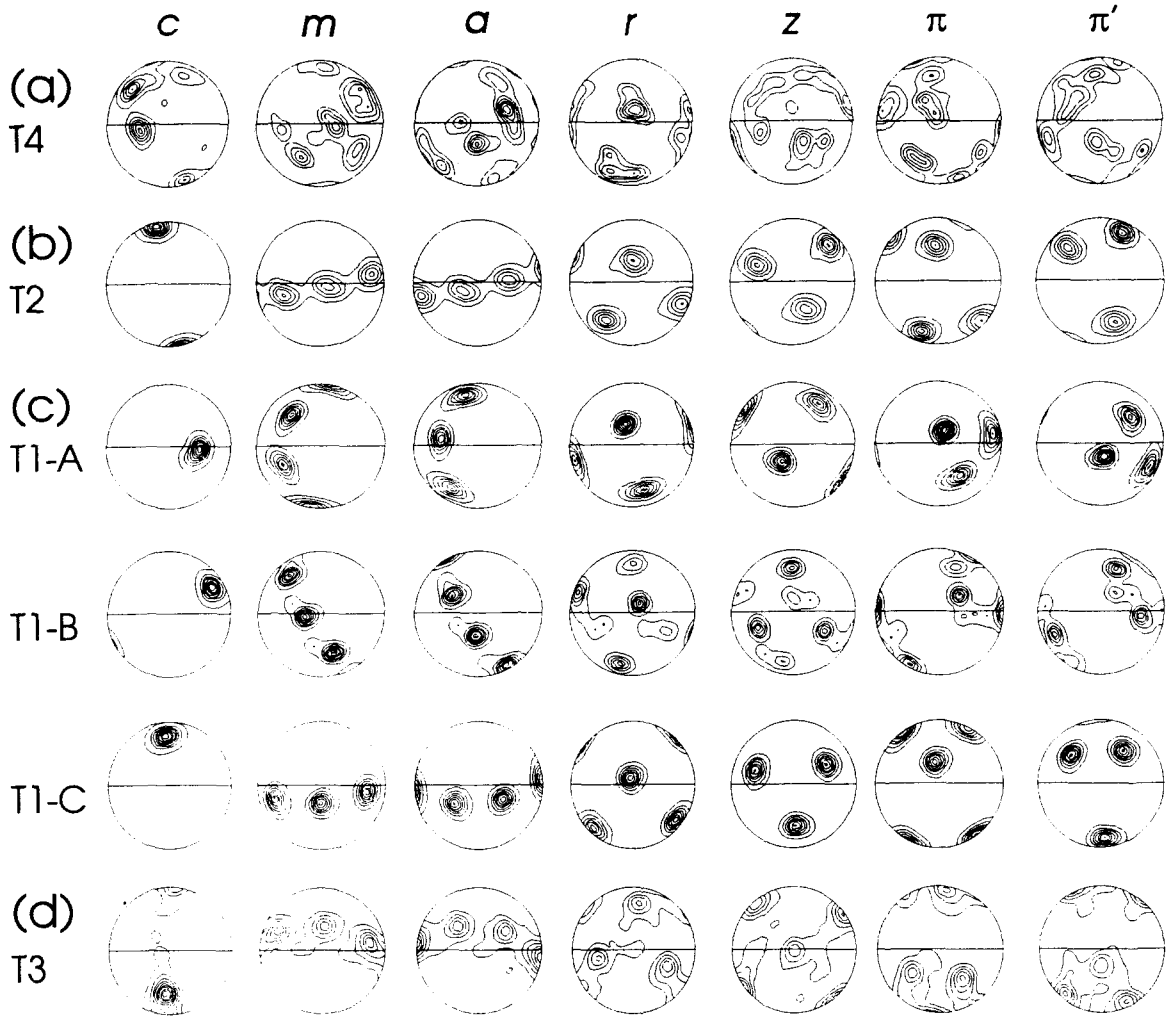

Fig. 8. Summary of crystal fabrics (contoured pole figures for c, m, a, r, z, π and π' crystal directions) from different parts of the shear zone (see Fig. 1b for locations) derived from ECPs (N, number of ECPs measured). Specimen co-ordinate system as for Fig. 1; minimum(interval)maximum contours measured in terms of multiples of uniform distribution. See text for discussion. (a) Shear zone margin (TORRID T4; see Fig. 1b) consisting of only ~14 grains ($N = 50$). Contours: c, 1(2)11; m, z, π, 1(1)4; a, 1(1)6; r, 1(1)5; π', 1(1)3. (b) Individual grain (TORRID T2; see also Fig. 3a) in the low to medium shear strain regions ($N = 213$). Contours: c, 1(5)40; m, a and r, 1(2)9; z and π, 1(2)11; π', 1(2)13. (c) The three low shear strain grains (T1–A,B,C) shown in Fig. 4. A contours ($N = 48$): c, 1(5)36; m and z, 1(2)13; a, 1(2)11; r, π and π', 1(2)15. B contours ($N = 7$): c, 1(5)36; m and a, 1(2)15; r, π and π', 1(2)11; z. 1(2)9. C contours ($N = 18$): c, 1(5)36; m, a, r, z, π and π', 1(2)13. (d) Mature mylonite (TORRID T3); see also Fig. 5 and compare with the fabrics determined by Law *et al.* (1990, fig. 1c.). Contours: c, 1(2)17; m, z, π and π', 1(1)5; a, 1(1)6; r, 1(1)4.

watching for significant changes in ECP configuration (typically >10°, although this does not mean that the orientations cannot still share a particular crystal direction—see below). These indicate the positions of grain boundaries. This approach reveals that the margin to the shear zone in this specimen, which has dimensions of ~15 mm in the X direction and ~7.5 mm parallel to Z, consists of only about 14 quartz grains (Fig. 1b). This is not surprising given that the shear zone developed from a vein within the gneissic host rock (Fig. 1a). Some grains, particularly those just within the shear zone, have intragranular features (e.g. subgrains, deformation bands, etc.) which result in some variability of grain orientation. We have therefore collected a range of ECPs from the grains to represent this variation in crystal orientation.

The crystal fabrics for the shear zone margin (T4) are shown in Fig. 8(a). The c-axis fabric can be considered in terms of two great-circle distributions which intersect in a maximum which lies close to the XZ plane at ~45° Z. The m-direction fabric can be considered in terms of three great-circle distributions with two intersections: one close to the XZ plane, <45° to X; the other in the XY plane close to Y. The a-axis fabric can also be considered in terms of three great-circle distribtions, but with a maximum defined by a single common intersection at ~20° to the XY plane, ~35° to X. The r fabric displays three (diffuse) clusters typical of a single crystal. In contrast, the z fabric consists of two components: a great-circle distribution and a (diffuse) point maximum. Similar configurations are shown by the fabrics of the corresponding π and π' directions.

Low to medium shear strain fabrics

Domino-style microstructures. We have already recognized these microstructures (e.g. Figs. 2 and 3) as being typical of low shear strain regions in this shear

zone. Detailed SEM/ECP analysis (Fig. 8b) of the region shown in Fig. 3a (T2) shows that the non-basal plane crystal fabrics define an approximate single crystal orientation. This supports our earlier observation that the domino microstructures are intragranular in origin. Furthermore, there has been only slight dispersions of crystal directions away from their original orientations in spite of the dramatic change in microstructure (and in particular grain–subgrain size). Indeed, the *c*-axis fabric is coincident with an orientation observed in the original fabric (compare Fig. 8a). It forms a pole, oriented subparallel to *Z*, to a great circle, oriented subparallel to the *XY* plane, defined by more dispersed and overlapping clusters of the *m* and *a* directions.

Because the deformation is intragranular and the deformed orientations shared similar original orientations, such crystal direction dispersion patterns can be interpreted (e.g. Lloyd & Freeman 1991) in terms of external rotation about the *c*-axis (and/or *Z*). Thus, *c* must lie within the slip plane and be perpendicular to the slip direction, which must therefore lie within the basal plane. This suggests that the domino-style microstructure in Fig. 3(a) has developed by slip on a prism plane. Unfortunately, the dispersion patterns do not provide sufficient information to determine the slip direction within the basal plane; this would require, for example, detailed knowledge of the orientation of subgrain walls, probably derived via transmission electron microscopy. Prism slip on $\{10\bar{1}0\}$ in an *a* direction has been commonly observed in quartz (e.g. Starkey 1979, Mancktelow 1987, Fueten *et al.* 1991), particularly at medium to high temperatures (Wenk *et al.* 1989, Wenk & Christie 1991), and would obviously meet the requirements described here.

The intragranular crystal fabrics (Fig. 9a) measured along a traverse parallel to *Z* in the direction of increasing shear strain (T2–X3; see Fig. 3a for location) effectively define a single crystal orientation (the subtle dispersions observed perhaps suggest crystal slip on a prism plane in a direction within the basal plane). However, the inverse pole figure of grain normal (parallel to specimen *Y*) directions exhibits ~60° spread of the data between two adjacent *m* directions. This difference can be explained by the traverse sampling different

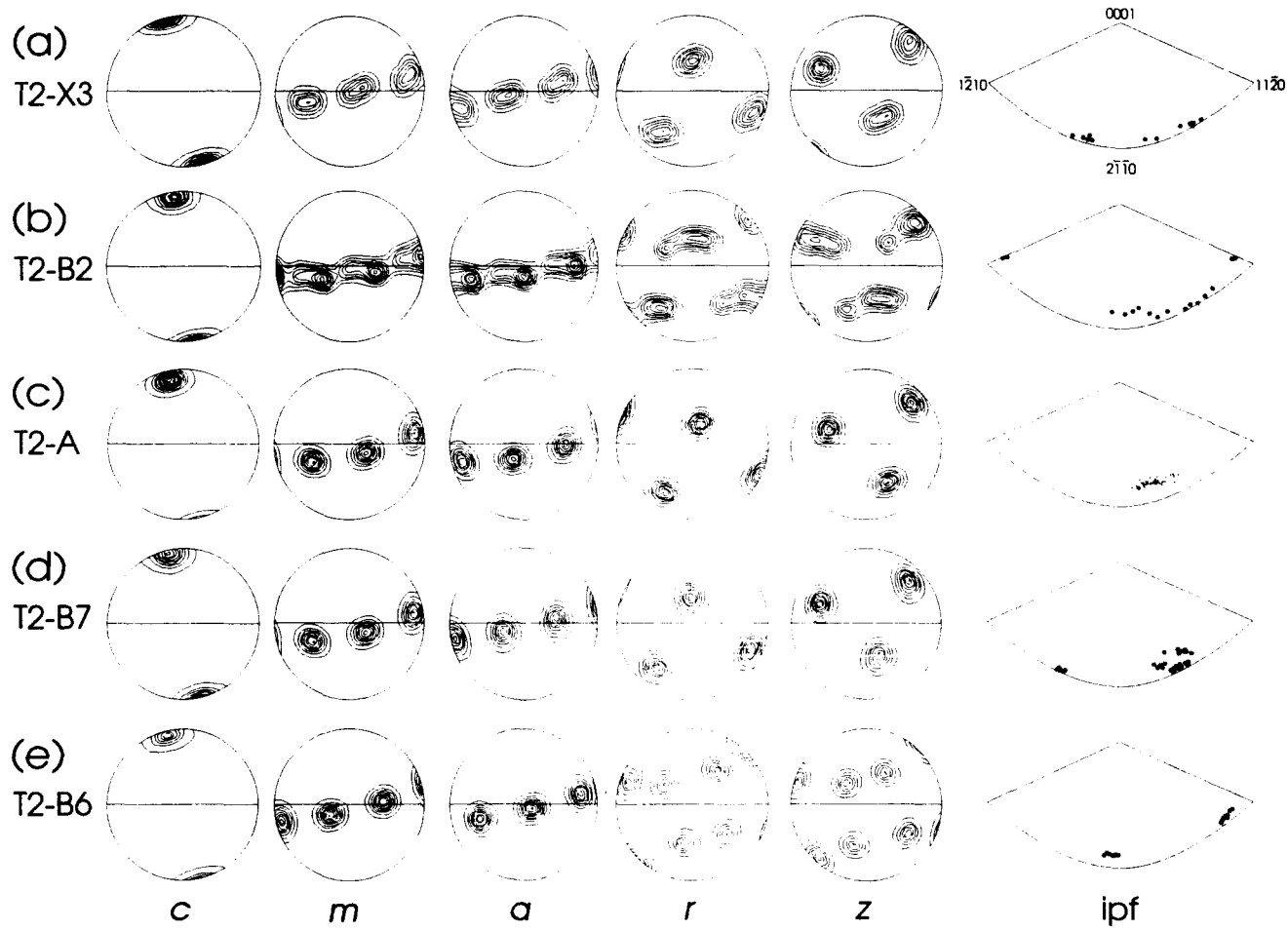

Fig. 9. Contoured pole figures and individual data inverse pole figures (ipf) for grain/ECP normal (specimen *Y* direction) derived from SEM/ECPs for different parts of TORRID T2 (Fig. 8b; see Fig. 3 for locations). Nomenclature as for Fig. 8; specimen co-ordinate system as for Fig. 1. See text for discussion. (a) T2–X3 (N=13): intragranular fabrics along a traverse parallel to *Z*. Contours: *c*, 1(5)51; *m* and *a*, 1(2)11; *r* and *z*, 1(2)13. (b) T2–B2 (N = 16): crystal fabrics for an individual band (elongate subgrain) between two adjacent linear boundaries. Contours: *c*, 1(5)46; *m* and *a*, 1(1)9; *r* and *z*, 1(1)7. (c) T2–A (N = 49): <20 μm grain size reduction (deformation localization) fabric along linear intragranular boundary between T2–B2 and T2–B7. Contours: *c*, 1(5)56; *m*, *a*, *r* and *z*, 1(2)15. (d) T2–B7 (N = 28): crystal fabrics for individual band (elongate subgrain) between two adjacent linear boundaries. Contours: *c*, 1(5)41; *m*, *a*, *r* and *z*, 1(2)15. (e) T2–B6 (N = 15): region suggestive of Dauphine twinning. Contours: *c*, 1(5)56; *m* and *a*, 1(2)17; *r* and *z*, 1(2)9.

microstructural domains, each with its own characteristic crystal slip system. Together these define an approximate single crystal orientation but also result in a dispersion of the grain normals between two adjacent *m* directions. We now test this hypothesis by considering the crystal fabrics of distinct intragranular microstructural domains recognized. However, it should be mentioned that both the pole and inverse pole figures for the intragranular traverse are consistent with the bulk external rotation about the specimen *Z* direction (i.e. out of the plane of section).

Individual domino fabrics. The significant microstructural modifications observed in individual grains at low shear strains due to the domino-style deformation (e.g. Figs. 2 and 3) do not appear to be reflected by major crystal fabric changes. However, if we consider an individual elongate subgrain, or domino, region (T2–B2; see Fig. 3a for location) this situation changes somewhat. The crystal fabrics (Fig. 9b) have more exaggerated dispersion patterns than for the whole grain (compare Fig. 8b), but still indicate the operation of a prism slip system. The inverse pole figure for the grain normal directions shows over 60° rotation about the *c*-axis within the basal plane between adjacent *a*-axes.

In contrast, the intragranular fabric associated with a nearby elongate subgrain or domino region (Fig. 9d, T2–B7; see Fig. 3a for location) defines almost a single crystal orientation. Any (subtle) dispersion observed appears to be confined to the $\{11\bar{2}0\}$ crystal plane subparallel to *YZ*. Such behaviour would imply rotation about the *a*-axis subparallel to *X* (or, about the *X* tectonic axis, out of the plane of the section), which must therefore lie within the slip plane and be perpendicular to the slip direction. Constraining the maximum dispersion to lie within a $\{11\bar{2}0\}$ prism plane means that the slip direction must also lie within the basal plane. The only direction which meets these demands is the *m* direction subparallel to *Y*. These relationships suggest that this particular microstructure has developed by slip on the basal plane in the *m* direction (e.g. Lloyd & Freeman 1991). Although this slip system has been recognized before, it is not favourable compared with others which are (potentially) available. It should also be noted that the inverse pole figure has two distinct groups of orientations centred on adjacent *a*-axes.

These observations suggest that deformation in different parts of the same grain is accommodated by crystal slip on different systems. Such behaviour demands that compatibility be maintained between the different elongate subgrain regions.

Inter-domino fabrics. The linear boundaries between adjacent elongate subgrains or dominoes are often marked by finer grain–subgrain sizes. SEM/ECP derived pole figures (Fig. 9c) for the boundary (T2–A) between subgrains T2–B2 and T2–B7 (see Fig. 3 for location) exhibit only very slight dispersions, similar to the T2–B7, and effectively define an approximate single crystal orientation. However, the inverse pole figure for the grain/ECP normal (specimen *Y* direction) does show dispersion, perhaps up to 30° between adjacent *a* and *m* directions (this is different to the pattern shown by T2–B7). These patterns are probably consistent with slip on a prism plane in a direction which lies within the basal plane.

The crystal direction dispersion patterns measured from the subgrains which decorate elongate subgrain boundaries are consistent with our earlier interpretation that these boundaries accommodate (localized) deformation. However, the patterns are not consistent with an interpretation of deformation accommodated by significant grain boundary sliding. This would tend either to maintain the original crystal direction orientations (i.e. due to rotation axes constrained to the grain normal, that is specimen *Y*, direction) or to induce random/irregular dispersion paths (i.e. due to unconstrained rotation axes).

Other intragranular fabrics. We now consider the intragranular crystal fabrics (Fig. 8c) of three adjacent grains (A, B and C) shown in Fig. 4 (see Fig. 1b for location) and described in the microstructural section. We have aldready recognized different behaviours in these grains.

The pole figures for Grain A (Fig. 8c, T1–A) show increasing dispersion of crystal directions from the centre of the figure (i.e. specimen *Y* direction) towards the primitive. This suggests that a crystal direction close to the centre of the pole figure has acted as an axis of rotation. In detail, it is either one of the three *r* or π directions which shows the least dispersion and therefore qualifies as the potential rotation axis. This axis must lie within the slip plane and be perpendicular to the slip direction, which is therefore constrained to be parallel to an *a*-axis. Such a configuration is consistent with either rhomb slip (e.g. $\{01\bar{1}1\}\langle 11\bar{2}0\rangle$) or acute rhomb slip (e.g. $\{10\bar{1}2\}\langle 11\bar{2}0\rangle$). The latter is the system postulated by Law *et al.* (1990).

We should mention that the Grain A fabrics are also consistent with rigid-body rotation of the grain about the specimen *Y* axis. This is supported by our earlier microstructural observations (see Fig. 4), in which we recognized that this particular grain exhibited a thin surface region, separated from the mantle subgrain region, by a narrow zone of concentrated deformation (shear band or deformation lamellae). We suggested that this region was being peeled off the rest of Grain A. Such a process would possibly induce rigid-body rotation of the whole grain.

The fabrics of Grain C (Fig. 8c, T1–C) can also be interpreted in terms of rhomb slip $\{01\bar{1}1\}\langle 11\bar{2}0\rangle$ (but probably not acute rhomb slip), although the dispertions about the *r*-axis subparallel to *Y* are less than those shown by Grain A. However, we have already seen (Fig. 4) that the microstructures of the two grains are different. Grain C occupies the 'pressure shadow region' adjacent to a feldspar fragment and has an alternating microstructure consisting of elongate (domino) subgrains and less well defined subgrains. This suggests

intragranular partitioning of deformation and/or the operation of different crystal slip systems.

The fabrics of Grain B (Fig. 8c, T1–B) show rotation about the *c*-axis and the initiation of a basal plane great-circle distribution. As we have already seen, this is consistent with prism slip in a direction constrained to lie in the basal plane (probably an *a*-axis). However, although both the *r*, *z* and π, π' fabrics support this interpretation, they each contain six rather than three orientation clusters within the overall dispersion pattern. Such distributions indicate the presence of Dauphine twinning.

Dauphine twinning fabrics. Dauphine twins cannot be distinguished optically because the *c*-axes in the host and twin are parallel, but this is inconsequential for SEM/EC analysis. The twinning represents a 180° rotation about the *c*-axis. However, because the quartz *c*-axis is a three-fold axis, it can also be described as a 60° rotation about *c*. It therefore interchanges the *r* and *z* directions, and the π and π' directions, resulting in the distributions observed in Fig. 8(c), T1–B.

Within each fabric there are three major and three minor clusters. The former could be interpreted as the host grain orientation and the latter as the twin orientation. However, it has been found experimentally that Dauphine twinning is activated by differential stress and results in a preferred orientation of the pole to *r* rhombs parallel to the compressional stress axis (Tullis & Tullis 1972, Tullis *et al.* 1973). This would mean that the major clusters represent the twin orientation and the minor clusters the host grain orientation. Furthermore, the *r* direction orientation maximum close to *Y* should therefore define the compressional stress axis. Interestingly, this is the only cluster to show no tendency for dispersion. Alternatively, the twinning in this grain could be attributed to compression parallel to all three major *r* clusters, which are almost equally developed as well as being approximately orthogonal.

The minor *r*, *z* and π, π' clusters show the most dispersions, whilst the major clusters are also the tightest (Fig. 8c, T1–B). We have already seen that prism slip operated elsewhere in this grain, which would account for the dispersion of the minor clusters. The fact that the major clusters do not show dispersion suggests that these orientations were not subjected to prism slip. This can be explained if these orientations did not exist when prism slip was operating in this grain, which supports the interpretation that the major clusters represent the twins. However, it also means that the Dauphine twins were produced during shear zone evolution, presumably by compression parallel to *r*, which suggests that they represent deformation twins. This contradicts traditional beliefs, which assume that no deformation (e.g. in the sense of calcite twins) of the crystal structure (i.e. a direct lattice shear) is caused by Dauphine twinning.

Dauphine twinning microstructures. We have clear microstructural evidence for Dauphine twins in SEM/EC orientation contrast images of several grains, although verification of the twin relationships depends on crystal orientation determination via ECPs. For example, although the grain shown in Fig. 3(a) is dominated by domino-style microstructures (involving basal and prism slip and perhaps localized recrystallization and grain boundary sliding), a small region (Fig. 6f; see Fig. 3a for location) shows a different microstructure consisting of alternating dark and bright EC orientation contrasts. The inverse pole figure of the grain/ECP normal directions (parallel to the specimen *Y* axis) for this region shows two groupings ~60° apart, whilst the pole figures show an interchange between the *r* and *z* directions (Fig. 9e). These observations are characteristic of Dauphine twinning.

A combination of ECP and orientation contrast analysis allows us to identify the host-grain and twin components in this microstructure (Fig. 6f). Two scales of twinning are clearly present, with the smaller scale host-twins penetrating between the larger scale host-twins. The upper, linear boundary to this penetration is oriented at ~45° to *XY* (and therefore to S_A), whilst the lower boundary is oriented at ~30° to *XY*, although it is more irregular. The boundaries between the smaller scale host-twins are subparallel to each other and to *YZ*.

We believe that there are three possible explanations for this Dauphine twinning microstructure. (1) The microstructure is suggestive of a penetration twin and may therefore be an original feature of the grain. (2) One of the three twin *r* orientations may represent the compression axis in this part of the grain, in which case these are deformation twins. (3) The microstructure also has the appearance of a healed crack-tip, with the smaller scale host-twins filling the crack void and growing epitaxially on to the larger scale host-twins with a coincident site lattice relationship (e.g. McClaren 1986). The irregular lower boundary to the 'crack' may therefore be due to local grain boundary migration into the more deformed (higher strain energy) original grain. This last explanation implies that shear zone evolution involved local stable (subcritical?) fracturing, and subsequent (concurrent?) fracture-healing with quartz via diffusion mass transfer processes, presumably from local sources.

It should also be mentioned that the overall dispersion patterns of the crystal directions in the pole figures (Fig. 9e) suggest rotation about the *c*-axis, consistent with prism slip.

High shear strain fabrics

Figure 8(d) shows the individual data and contoured pole figures measured from the high shear strain (mylonitic) part of the shear zone (Fig. 5, T3; see Fig. 1b for location). They show an almost single crystal symmetry, which may have significant implications for fabric evolution (see below). In general, they are in broad agreement with those measured by Law *et al.* (1990) (see Fig. 1c), although in detail these workers recognized two single crystal orientations sharing a common *a*-axis orientation slightly inclined to *X*. However, interpre-

tation of the SEM/EC derived fabrics is not necessarily straightforward because we can also recognize slight dispersions away from the single crystal orientation.

Our measurements show a somewhat weaker single girdle *c*-axis distribution than Law *et al.* (1990) found; the girdle is not continuous and there is a tendency towards a *c*-axis maximum close to the *YZ* plane, ~30° to *Z*. The other crystal directions exhibit maxima in their distributions but also show a tendency towards weak dispersions away from these orientations. However, because the grains from which these orientations were measured are not necessarily derived from the same parental grain (indeed, it is usually assumed that mylonitic fabrics develop from many parental grains), we cannot *a priori* interpret the dispersion patterns in terms of the operation of specific crystal slip systems, as we have done previously. But, the slight dispersions observed in the fabrics are away from the apparent single crystal orientation, which therefore presumably represents a (slightly) earlier stage in the fabric evolution. Thus, we perhaps are justified in using these dispersion patterns to deduce crystal slip systems valid for the last stage in the fabric evolution.

Some of the dispersions (e.g. the tendency towards a basal plane girdle distribution and the small circle π' distribution) can be accounted for by rotation about the *c*-axis maximum and hence prism slip. However, there is a suggestion of dispersion out of the basal plane, as well as dispersion of the *c*-axes towards a girdle distribution subparallel to *YZ*. Both can be accounted for by rotation about the *a*-axis subparallel to *X* and therefore basal plane slip parallel to an *m* direction. There is also suggestion of rotation about the *z* direction oriented in the *XZ* plane at ~45° to *Z*, which would be explained by rhomb slip (presumably parallel to *a*). Finally, there is a hint of three minor groups of orientations in the *r* and *z* pole figures consistent with Dauphine twinning (note: Law *et al.* 1990, also measured this trend).

Thus, it appears that we may have sampled in the fabric evolution close to, but not quite at, the final stage detected by Law *et al.* (1990). For example, the weak dispersion away from the *c*-axis point maximum can be interpreted in terms of development towards the single girdle subparallel to *YZ* measured by them (see Fig. 1c). However, the origin of the apparent single crystal orientation from which these dispersions develop, and its role in the formation of the entire shear zone, are more problematic.

SHEAR ZONE FORMATION

In this section we derive the deformation path responsible for shear zone formation. Initially, we are concerned with establishing the crystal fabric evolution path(s) between the shear zone margin fabric (Fig. 8a) and the mature mylonitic fabric (Fig. 8d). This is achieved via information gained from intermediary, low to medium shear strain fabrics (Figs. 8b&c and 9) and relevant microstructural observations (Figs. 2–6).

Crystal fabric evolution

Observed fabrics and slip systems. We again emphasize that the original crystal fabric (which comprises only 14 grains) is typical only of the sample studied. Other regions of the shear zone margin are likely to have inherited different fabrics. Together, these represent the parental fabric for the whole-rock mylonitic shear zone. Although both the initial and final fabrics show a tendency towards single crystal distributions, we have observed no obvious common elements in, or crystal direction dispersion paths between, the initial and final fabrics (Fig. 8).

Evidence for the crystal slip systems which operated during shear zone formation is provided by the low-to-medium and high shear strain crystal fabrics. These can be interpreted in terms of slip on prism, basal, rhomb and acute rhomb planes, with the slip direction constrained to lie in the basal plane (presumably parallel to *a* and/or *m*). In addition, there is evidence for rigid-body rotation about all three specimen axes (i.e. *X*, *Y* and *Z*) and hence for movement out of the *XZ* plane during shear zone formation. Significant syn-deformation Dauphine twinning has also occurred.

Law *et al.* (1990) argued that the simple relationships between crystal fabrics and shear zone geometry and kinematics observed in the mature shear zone supported the formation of the crystallographic fabric by a single internally consistent mechanism rather than by the superimposition of fabric elements due to several slip systems. They identified acute rhomb [*a*] slip because of the preferential alignment of one potential (π')[*a*] system in most grains. We have only indentified (π') [*a*] as a potential crystal slip in one isolated case via SEM/ECP analysis. However, Law *et al.* (1990) admitted that simultaneous basal ⟨*a*⟩ and negative rhomb (*z*)⟨*a*⟩ slip could also be responsible, with other fabric elements being produced by Dauphine twinning. Our observations have recognized each of these processes, as well as several others.

Unfortunately, the fact remains that the crystal fabrics measured for the mylonitic shear zone, both by ourselves and Law *et al.* (1990), have little in common with any of the fabrics described from the low-medium shear strain or shear zone margin regions. Given the spread of orientations present in the initial fabric (Fig. 8a), *it is extremely unlikely* that a single crystal slip mechanism could *efficiently* achieve the almost single crystal-like fabric (Fig. 8d) of the mature shear zone. However, the mature shear zone does appear to be behaving as a single crystal, such that a single slip system could perhaps operate efficiently to accommodate the necessary deformations at high shear strains. We believe that the apparent single crystal orientation of the mature shear zone can be explained either by inhomogeneous deformation of many original grains or by deformation of a single, large original grain.

Inhomogeneous deformation. Inhomogeneous deformation of many original grains on different slip systems

could eventually achieve common crystal directions which define a single crystal orientation. We have certainly recognized considerable evidence for inhomogeneous deformation, both within and between grains. However, shear zone fabrics generally consist of a preferred directional orientation rather than a preferred single crystal orientation. That many different original grains should strive to reach the same crystal orientation suggests that there must be something very special about this orientation, in which case we would expect to have found it in other shear zones. Alternatively, it is possible that a single crystal can accommodate more efficiently the necessary deformations involved in the shear zone, but again there is little supportive evidence for this. Furthermore, such behaviour would presumably promote significant grain growth to achieve the single crystal orientation over as big a volume of rock as possible.

If a single crystal orientation can be achieved by the inhomogeneous deformation of many grains, the shear zone can then attempt to deform homogeneously on a single, preferred slip system. However, such behaviour will not preserve all the single crystal orientations because even a preferred slip system must induce rotations about the external direction parallel to the slip plane normal. For example, prism slip constrains a stable *c*-axis orientation about which the other directions rotate or disperse on great and small circles. This means that shear zones should not be able to maintain completely stable crystal fabrics and any fabric measured represents the latest to develop at a specific location (see also Wenk *et al.* 1989, Wenk & Christie 1991). We have recognized a tendency towards dispersions away from the single crystal orientation in the mature shear zone fabric (Fig. 8d) which might be indicative of this behaviour.

The stability of a single crystal orientation during continued deformation demands that some other process operates to continually bring the grains back into this orientation. The most obvious candidate is dynamic recrystallization. Wenk & Christie (1991) have emphasized that dynamic recrystallization is a major process by which preferred orientation can develop due to the preferential selection of grains with low internal strain energies which therefore continue to dominate the fabric. However, we have only observed evidence for local dynamic recrystallization in the mature shear zone microstructure.

We should also mention that grain boundary sliding (for which we have observed some local evidence) could maintain a constant crystal fabric if it only involved the *translation* of individual grains relative to each other. However, this is extremely unlikely and individual rotations (about many axes) are probably necessary to maintain compatibility. Such behaviour is likely to randomize any fabric. Even rotation about a single common axis (say parallel to *Y*) would only result in the preservation of a fabric element parallel to this external axis; all other elements would migrate along small circle dispersion paths.

Single parental grain. We have already seen that the shear zone margin consists of about 14 large grains (Fig. 1b) which exhibit significant microstructural changes (e.g. Fig. 3a) whilst maintaining many of their original crystal fabric elements (Figs. 8b and 9). Futhermore, as the shear strain gradient develops we have observed the presence of discrete microstructural domains with sharp boundaries which often truncate against each other (e.g. Figs. 2 and 6). We have interpreted these features as representing the persistence of original (including grain boundaries) and lower shear strain features to higher shear strains. Thus, how much of the mature mylonitic shear zone can be achieved by the deformation of an individual original grain?

Examination of the SEM specimen (Fig. 1b) suggests that the mature mylonite occupies only $\sim 5 \times 17 = 85$ mm^2 (including some feldspar) and consists of grains typically $20 \times 10 = 200\ \mu m^2$ in size (e.g. Figs. 5 and 6c–e). This means that there are about 4.25×10^5 recrystallized quartz grains in the specimen mylonite. We saw earlier that grains in the shear zone margin can be large. If we therefore assume that an original grain at the margin can be represented by a square element of maximum dimensions $5 \times 5 = 25$ mm^2 (or minimum $1 \times 1 = 1\ mm^2$), then the number of recrystallized grains it can produce is between 1.25×10^5 and 5×10^3. Thus, only between 3.4 and 85 original grains are needed to produce the mature mylonite grain structure of this specimen. If we take this argument a stage further and allow out-of-section movement (remember, there is crystal fabric evidence to suggest rotation occurs about the *X*, *Y* and *Z* specimen axes), the original grain can now be represented by a cubic element of maximum dimensions $5 \times 5 \times 5 = 125$ mm^3 and minimum $1 \times 1 \times 1 = 1\ mm^3$. In the extreme case, where the out-of-section movement reduces this dimension for the original grain to that of a typical recrystallized grain (say 10 μm), this produces between 6.25×10^8 and 5×10^6 recrystallized grains. The mature mylonite grain structure can now be produced by only 6.8×10^{-4} (or 0.085) original grains!

Mylonite fabric evolution. Based on the above arguments, it is conceivable for the mature mylonite in the specimens considered both here and by Law *et al.* (1990) to have been produced by the deformation of a single grain, or a few grains. Although the measured mylonite fabric is not recognized at lower shear strains, this merely means that the grain orientation which formed this part of the mylonite was not represented in either our original (which consisted of only 14 grains) or intermediary fabrics. However, the mylonitic fabric can only display an approximate single crystal orientation if the fabric evolution path, and associated crystal slip systems, were homogeneous for all parts of the parental grain throughout the deformation history. We have observed that inhomogeneous deformation, resulting in a variety of microstructures, can be accomplished with-

out significant change in the crystal fabric, so this is not a problem.

Thus, the interpretation of a single dominant slip system for mylonite development (e.g. Law *et al.* 1990) based on a characteristic mylonitic fabric is not surprising. However, it does not mean that this system operated universally throughout the shear zone, or that it operated continuously in this part of the shear zone. The observed orientation can be regarded as representing a specific step along a continuous fabric migration path. At any instant, the fabric is migrating away from one single crystal orientation towards some other single crystal orientation along a path determined by the specific crystal slip system(s) operating. This progressive change in single crystal orientation may lead to the operation of a different slip system, which in turn leads to some other system. The observed (instantaneous) fabric, and the crystal slip system(s) deduced, are consequently not necessarily representative of the whole fabric history. This supports the idea, mentioned above, that shear zones are unable to maintain completely stable crystal fabrics and any fabric measured merely represents the latest to develop at a specific location. Determination of fabric evolution paths via the measurement of fabrics at different shear strains, rather than the finite shear strain fabric alone, is therefore crucial to the determination of shear zone deformation paths and histories. Thus, if crystal fabric evolution paths can be established across shear zones, it may be justified in considering them as representing true time gradients.

Shear zone evolution

Our microstructural (Figs. 3–6) and crystal fabric (Figs. 8 and 9) observations support the following interpretation for the evolution of the Torridon shear zone. This interpretation is illustrated schematically in Fig. 10 (based on the linear SEM/EC orientation traverse across the shear zone shown in Fig. 2), which shows the progressive microstructural development of the shear zone from the margin, through low to medium shear strains, to the high shear strain mature mylonite.

We consider that the mature shear zone consists of a series of deformed shear zone margin grains stacked on top of each other in a manner which preserves original grain boundaries as well as the intragranular features which developed during shear zone evolution. This is perhaps analogous to *transition bands* found in highly deformed metals, which form at the boundaries between different parts of the same grain that have undergone different rotations during deformation by use of a different combination of crystal slip systems to achieve the imposed strain (e.g. Haessner 1978). Intragranular deformation, particularly early in the shear zone evolution (i.e. at low shear strains), has been accommodated mainly by crystal slip on several different systems, although the significance of Dauphine twinning has also been recognized. These systems involve slip parallel to prism, basal and rhomb crystallographic planes, in crystal directions lying within the basal plane (probably parallel to *a* and/or *m*). This results in considerable microstructural variation, including significant grain size reduction. Grain size reduction by dynamic recrystallization, and grain boundary sliding have locally assisted in deformation accommodation within and between grains by maintaining mechanical compatibility, leading to further microstructural variation and perhaps significant movement out of the XZ plane of section.

The different crystal slip systems or processes operate within individual grains to produce a similar, mylonitic microstructure. However, the crystallographic orientations only locally define an approximate single crystal. This region corresponds to either all or part of an original parental grain. Such a region is obviously capable of responding as a single crystal to accommodate more efficiently further shear strain by the operation of a specific slip system (e.g. $(\pi')[a]$ slip, as suggested by Law *et al.* 1990). As deformation continues, the single crystal regions become progressively narrower parallel to Z and elongate parallel to X. This deformation can be accommodated by further crystal slip (abetted by local dynamic recrystallization and/or grain boundary migration). However, because the mylonitic grain size is now small (typically <20 μm), grain boundary sliding processes may also become important. Deformation compatibility between adjacent regions with different single crystal orientations is accommodated by the development of shear bands parallel to S_A.

Although the mylonitic grain size is capable of promoting diffusive mass transfer processes, we have found little evidence for these. Similarly, fracture processes (and in particular cataclasis) have not been identified. The interpretation of the Dauphine twinning microstructure in Fig. 6(f) as a healed microcrack remains only an interesting possibility.

Thus, although the crystallographic fabric of the mature shear zone may exhibit the bulk simple shear kinematic framework indicated by shear zone geometry, the deformation path followed during shear zone evolution may depart significantly from simple shear. In particular, the early stages of shear zone development would appear to involve significant out-of-section displacement to accommodate the incompatibilities which must naturally exist, especially on the scale of the initial grain size.

CONCLUSIONS

(1) The scanning electron microscope operated in the electron channelling mode has been used to investigate the microstructures (via orientation contrast) and crystal fabrics (via electron channelling patterns) of a quartzofeldspathic shear zone developed in a vein in Proterozoic gneiss from Torridon, NW Scotland.

(2) Although the margin to the shear zone consists of only about 14 grains, a variety of microstructures, which

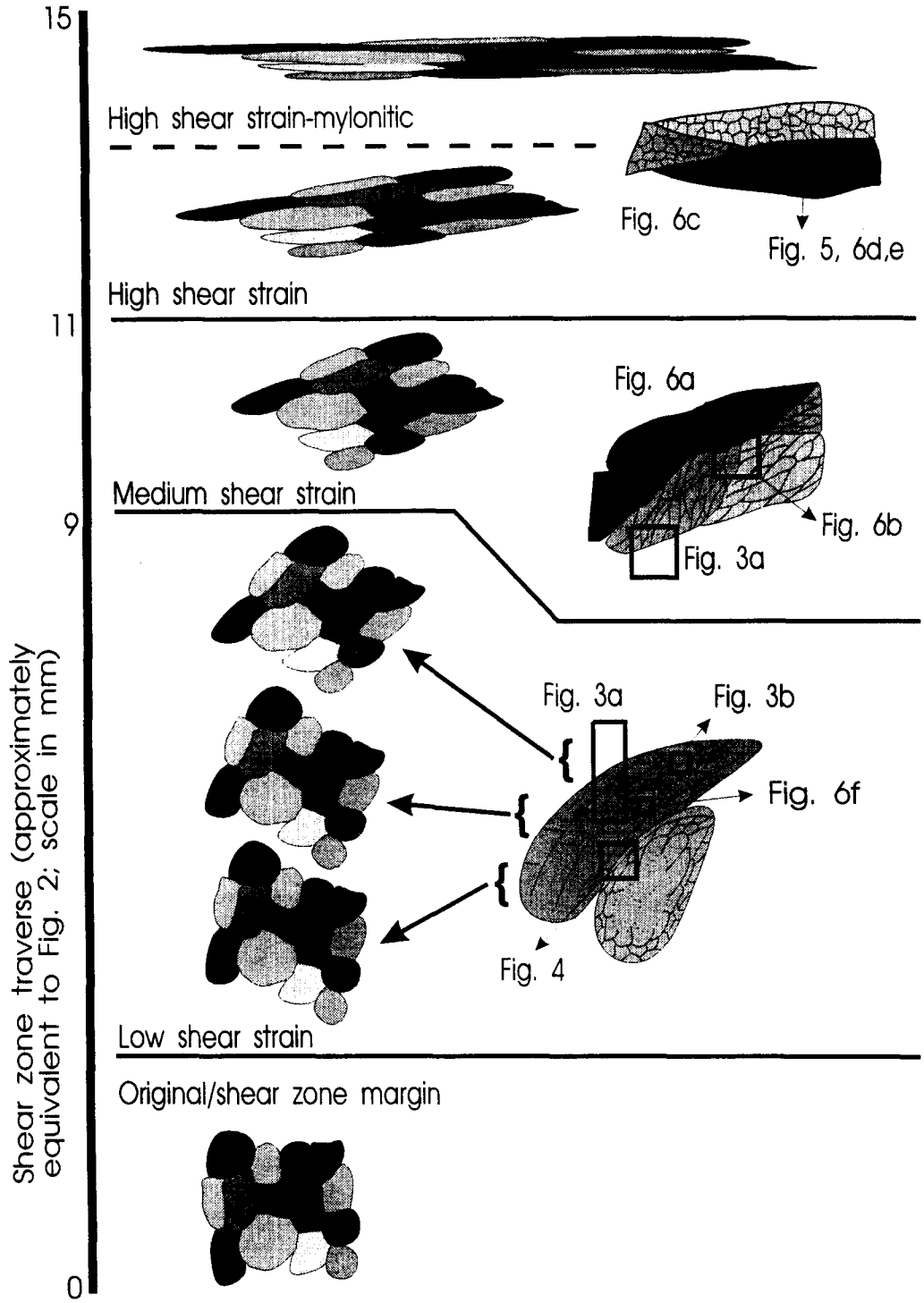

Fig. 10. Schematic interpretative linear traverse across the Torridon shear zone, illustrating its microstructural evolution and formation. Based on the actual SEM/EC orientation contrast traverse shown in Fig. 2 (the approximate millimetric scale on the left edge allows comparison) and observations made in Figs. 3–6 (as indicated). The left-hand side shows the progressive microstructural development from margin shear zone, through low to medium shear strains, to the high shear strain mature mylonite. The right-hand side shows specific microstructural detail. The mature shear zone consists of a series of deformed initial grains stacked on top of each other in a manner which preserves both the original grain boundaries and intragranular features developed during shear zone evolution. Crystal fabric measurements suggest that different slip systems operated in each grain to produce a microstructure with a common *local* crystallographic orientation capable of responding as a single crystal to accommodate large finite shear strains by the operation of a single slip system. Thus, the local deformation path followed must depart significantly from simple shear and may involve significant out-of-section displacements. See text for full description.

change with increasing shear strain, have been recognized. Microstructural variation is particularly pronounced at low shear strains. Intragranular domino-style displacements are common, resulting in the development of both elongate and equant subgrains and eventually in grain size reduction. Other grains show core-and-mantle subgrain microstructure. The grain boundary regions between adjacent grains exhibit

characteristic deformation accommodation microstructures.

(3) A sudden reduction in grain size defines the transition to medium shear strains. However, both the inter- and intra-granular boundaries inherited from the original and low shear strain regions can still be recognized and define distinctive bands oriented at low but different angles to the shear zone margin. Grains within these bands have preferred but different dimensional orientations, somewhat steeper than their associated bands.

(4) The high shear strain region has a mylonitic microstructure with an approximately uniform sub-20 μm grain size. The grains occur within domains, defined by boundaries inherited from lower shear strains, oriented subparallel to the shear zone margin. The grains within these domains have a somewhat steeper preferred dimensional orientation. Localized, narrow deformation bands are also recognized, oriented parallel to the shear zone margin.

(5) The observed microstructures suggest that the principal deformation mechanism involved in shear zone formation was intracrystalline plasticity. However, contributions from grain size reduction via dynamic recrystallization, grain boundary migration and grain boundary sliding are also recognized. Only equivocal evidence was found for either diffusive mass transfer or fracture processes.

(6) Crystal fabrics measured from the shear zone vary with position, depending on the shear strain involved. The initial fabric is ill-defined due to the small number of relatively large grains present in the SEM specimen. Nevertheless, the fabrics as a whole are consistent with the operation of several crystal slip systems (i.e. slip on prism, basal, rhomb and acute rhomb planes in a consistent direction, probably parallel to *a* and/or *m*) rather than the dominance of a single system (e.g. $(\pi')[a]$ slip). They also reveal the presence of Dauphine twinning and suggest that this may be a significant process in quartz deformation.

(7) We have failed to find a single crystal fabric evolution path which links the shear zone margin fabric with the mature shear zone mylonitic fabric. Rather, the mylonitic fabric reflects the instantaneous fabric to develop at a particular location for a particular shear strain, and depends on the specific original parental grain orientation responsible for the microstructure *at that location*. However, if a crystal fabric evolution path (including high shear strain components due to recovery processes such as dynamic recrystallization, grain boundary migration and grain coalescence) can be established across a shear zone, it is likely to be equivalent to complete time and strain gradients of shear zone formation.

(8) The mature shear zone consists of a series of deformed shear zone margin grains stacked on top of each other in a manner which preserves original grain boundaries and intragranular features which develop during shear zone evolution. The stability of some microstructures to higher shear strains, together with the exploitation of others at lower shear strains, means that the strain gradient observed across many shear zones is unlikely to be equivalent to a time gradient. Furthermore, any time gradient component which is observed will stop with the development of a stable high shear strain (mylonitic) microstructure capable of accommodating further shear strains without modification.

(9) The stability of some microstructural elements and the instability of crystal fabrics and slip systems, which together mean that grains are capable of remembering only part of their earlier dispositions and characteristics (including perhaps parental allegiances), are likely to be important concepts in our understanding of the development of high shear strain and/or mylonite zones. The present study highlights the importance of SEM electron channelling analysis to these investigations.

Acknowledgements—We are grateful to CamScan plc (in particular Dick Paden) for producing an SEM capable of the type of analysis presented here. Neils-Henrik Schmidt provided upgrades when necessary of his CHANNEL ECP indexing program. Ian and Carol McNulty helped with computing facilities for GEL. This work was financed by the U.K. NERC (G. E. Lloyd, R. D. Law and J. Wheeler) and French CNRS (G. E. Lloyd and D. Mainprice), whilst an Anglo-French *Alliance* Award supported attendance (G. E. Lloyd) at the Montpellier conference on *Mechanical Instabilities*. Logistical assistance was provided by the University of Leeds. We are particularly grateful to the Journal's referees, Stefan Schmid and Jan Tullis, for their detailed comments which helped to produce the final version of this manuscript.

REFERENCES

Bouchez, J.-L. 1978. Preferred orientations of quartz a-axes in some tectonites: kinematic inferences. *Tectonophysics* **49**, T25–T30.

Bouchez, J.-L., Dervin, P., Mardon, J. P. & Englander, M. 1979. La diffraction neutronique appliquee a l'etude de l'orientation preferentielle de reseau dans les quartzites. *Bull. Mineral.* **102**, 231–255.

Burg, J.-P. & Laurent, P. 1978. Strain analysis of a shear zone in a granodiorite. *Tectonophysics* **47**, 15–42.

Etchecopar, A. 1977. A plane kinematic model of progressive deformation in a polycrystalline aggregate. *Tectonophysics* **39**, 121–139.

Freund, R. 1974. Kinematics of transform and transcurrent faults. *Tectonophysics* **21**, 93–134.

Fueten, F., Robin, P.-Y. F. & Stephens, R. 1991. A model for the development of a domainal quartz *c*-axis fabric in a coarse-grained gneiss. *J. Struct. Geol.* **13**, 1111–1124.

Haessner, F. 1978. *Recrystallization of Metallic Materials*. Dr. Riederer, Stuttgart.

Hanmer, S. & Passchier, C. 1991. Shear-sense indicators: a review. *Geol. Surv. Pap. Can.* **90-17**.

Joy, D. E., Newbury, D. E. & Davidson, D. L. 1982. Electron channelling patterns in the scanning electron microscope. *J. Appl. Phys.* **53**, R88–R122.

Law, R. D. 1987. Heterogeneous deformation and quartz crystallographic fabric transitions: natural examples from the Moine thrust zone at the Stack of Glencoul, northern Assynt. *J. Struct. Geol.* **9**, 819–833.

Law, R. D., Casey, M. & Knipe, R. J. 1986. Kinematic and tectonic significance of microstructures and crystallographic fabrics within quartz mylonites from the Assynt and Eriboll regions of the Moine thrust zone, NW Scotland. *Trans. R. Soc. Edinb., Earth Sci.* **77**, 99–126.

Law, R. D., Knipe, R. J. & Dayan, H. 1984. Strain path partitioning within thrust sheets: microstructural and petrofabric evidence from the Moine thrust zone at Loch Eriboll, northwest Scotland. *J. Struct. Geol.* **6**, 477–497.

Law, R. D., Schmid, S. M. & Wheeler, J. 1990. Simple shear deformation and quartz crystallographic fabrics: a possible natural

example from the Torridon area of NW Scotland. *J. Struct. Geol.* **12**, 29–45.

Lister, G. S. & Williams, P. F. 1983. The partitioning of deformation in flowing rock masses. *Tectonophysics* **92**, 1–33.

Lloyd, G. E. 1987. Atomic number and crystallographic contrast images with the SEM: a review of backscattered electron techniques. *Mineral. Mag.* **51**, 3–19.

Lloyd, G. E. & Ferguson, C. C. 1986. A spherical electron channelling pattern map for use in quartz petrofabric analysis. *J. Struct. Geol.* **8**, 517–526.

Lloyd, G. E., Ferguson, C. C. & Law, R. D. 1987a. Discriminatory petrofabric analysis of quartz rocks using SEM electron channelling. *Tectonophysics* **135**, 243–249.

Lloyd, G. E. & Freeman, B. 1991. SEM electron channelling analysis of dynamic recrystallization in a quartz grain. *J. Struct. Geol.* **13**, 945–953.

Lloyd, G. E., Law, R. D. & Schmid, S. M. 1987b. A spherical electron channelling pattern map for use in quartz petrofabric analysis: correction and verification. *J. Struct. Geol.* **9**, 517–526.

Lloyd, G. E., Schmidt, N.-H., Mainprice, D. & Prior, D. J. 1991. Crystallographic textures. *Mineral. Mag.* **55**, 331–345.

Mandl, G. 1987. Tectonic deformation by rotating parallel fault blocks: the "bookshelf" mechanism. *Tectonophysics* **141**, 277–316.

Mancktelow, N. S. 1987. Atypical textures in quartz veins from the Simplon Fault zone. *J. Struct. Geol.* **9**, 995–1006.

McClaren, A. C. 1986. Some speculations on the nature of high-angle grain boundaries in quartz rocks. In: *Mineral and Rock Deformation, Laboratory Studies—The Paterson Volume* (edited by Hobbs, B. E. & Heard, H. C.). *Am. Geophys. Un. Geophys. Monogr.* **36**, 233–246.

Platt, J. P. & Behrmann, J. H. 1986. Structures and fabrics in a crustal scale shear zone, Betic Cordilleras, SE Spain. *J. Struct. Geol.* **8**, 15–34.

Ramsay, J. G. 1967. *Folding and Fracturing of Rocks*. McGraw-Hill, New York.

Ramsay, J. G. 1980. Shear zone geometry: a review. *J. Struct. Geol.* **2**, 83–100.

Ramsay, J. G. & Graham, R. H. 1970. Strain variation in shear belts. *Can. J. Earth Sci.* **7**, 786–813.

Schmid, S. M. 1982. Microfabric studies as indicators of deformation mechanisms and flow laws operative in mountain building. In: *Mountain Building Processes* (edited by Hsu, K. J.). Academic Press, London, 95–110.

Schmid, S. M. & Casey, M. 1986. Complete fabric analysis of some commonly observed quartz *c*-axis patterns. In: *Mineral and Rock Deformation, Laboratory Studies—The Paterson Volume* (edited by Hobbs, B. E. & Heard, H. C.). *Am. Geophys. Un. Geophys. Monogr.* **36**, 263–286.

Schmidt, N.-H. & Olesen, N. O. 1989. Computer-aided determination of crystal-lattice orientation from electron-channelling patterns in the SEM. *Can. Mineral.* **27**, 15–22.

Simpson, C. 1981. Ductile shear zones: a mechanism of rock deformation in the orthogneiss of the Maggia Nappe, Ticino. Unpublished Ph.D. thesis, ETH, Zurich.

Starkey, J. 1979. Petrofabric analysis of Saxony Granulites by optical and X-ray diffraction methods. *Tectonophysics* **58**, 201–219.

Tullis, J., Christie, J. M. & Griggs, D. T. 1973. Microstructures and preferred orientations of experimentally deformed quartzites. *Bull. geol. Soc. Am.* **84**, 297–314.

Tullis, J. & Tullis, T. E. 1972. Preferred orientation produced by mechanical Dauphine twinning: thermodynamics and axial experiments. In: *Flow and Fracture of Rocks* (edited by Heard, H. C., Borg, I., Carter, N. & Raleigh, C.). *Am. Geophys. Un. Geophys. Monogr.* **16**, 67–82.

Wenk, H.-R., Canova, G., Molinari, A. & Kochs, U. F. 1989. Viscoplastic modelling of texture development in quartzite. *J. geophys. Res.* **94**, 17895–17906.

Wenk, H.-R. & Christie, J. M. 1991. Review Paper—Comments on the interpretation of deformation textures in rocks. *J. Struct. Geol.* **13**, 1091–1110.

Wenk, H.-R., Johnson, G. C. & Matthies, S. 1988. Direct determination of physical properties from continuous orientation distributions. *J. Appl. Phys.* **63**, 2876–2879.